

Original Research

Core Ideas

- Subsurface gas migration results in localized surficial CH₄ releases.
- Surficial CH₄ emissions show pronounced temporal variations.
- Methane concentrations in soil gas exceed lower explosive limits at low leakage rates.
- Increasing CO₂ effluxes and stable C isotope signatures indicate vadose zone CH₄ oxidation.
- Instantaneous surficial effluxes do not indicate the magnitude of subsurface gas leakage rates.

O.N. Forde, K.U. Mayer, and A.G. Cahill, Dep. of Earth, Ocean and Atmospheric Sciences, Univ. of British Columbia, 2007 Main Mall, Vancouver, BC, V6T 1Z4, Canada; B. Mayer, Dep. of Geoscience, Univ. of Calgary, 2500 University Drive NW, Calgary, AB, T2N 1N4, Canada; A.G. Cahill, J.A. Cherry, and B.L. Parker, G360 Institute for Groundwater Research, College of Engineering & Physical Sciences, Univ. of Guelph, 50 Stone Road East, Guelph, ON, N1G 2W1, Canada. *Corresponding author (oforde@eos.ubc.ca).

Received 19 Feb. 2018.
Accepted 15 July 2018.
Supplemental material online.

Citation: Forde, O.N., K.U. Mayer, A.G. Cahill, B. Mayer, J.A. Cherry, and B.L. Parker. Vadose zone gas migration and surface effluxes after a controlled natural gas release into an unconfined shallow aquifer. *Vadose Zone J.* 17:180033. doi:10.2136/vzj2018.02.0033

© Soil Science Society of America.
This is an open access article distributed under the CC BY-NC-ND license (<http://creativecommons.org/licenses/by-nc-nd/4.0/>).

Vadose Zone Gas Migration and Surface Effluxes after a Controlled Natural Gas Release into an Unconfined Shallow Aquifer

O.N. Forde,* K.U. Mayer, A.G. Cahill, B. Mayer, J.A. Cherry, and B.L. Parker

Shale gas development has led to concerns regarding fugitive CH₄ migration in the subsurface and emissions to the atmosphere. However, few studies have characterized CH₄ migration mechanisms and fate related to fugitive gas releases from oil or gas wells. This paper presents results from vadose zone gas and surface efflux monitoring during a natural gas release experiment at Canadian Forces Base Borden, Alliston, Ontario, Canada. Over 72 d, 51 m³ of natural gas (>93% CH₄) was injected into a shallow, unconfined sand aquifer at depths of 4.5 and 9 m. Methane and CO₂ effluxes in combination with soil gas concentrations and stable C isotopic signatures were used to quantify the spatiotemporal migration and fate of injected gas. Preferential gas migration pathways led to vadose zone hot spots, with CH₄ concentrations exceeding the lower explosive limit (5% v/v). From these hot spots, episodic surface CH₄ effluxes (temporally exceeding 2500 μmol m⁻² s⁻¹ [3465 g m⁻² d⁻¹]) occurred during active injection. Higher injection rates led to increased average CH₄ effluxes and greater lateral migration, as evidenced by a growing emission area approaching 25 m² for the highest injection rate. Reactive transport modeling showed that high CH₄ fluxes resulted in advection-dominated migration and limited CH₄ oxidation, whereas lower CH₄ effluxes were diffusion dominated with substantial CH₄ oxidation. These results and our interpretations allowed us to develop a conceptual model of fugitive CH₄ migration from the vadose zone to the ground surface.

Abbreviations: CFB, Canadian Forces Base; GM, gas migration; RTM, reactive transport model; VWC, volumetric water content.

The rise in shale gas development has heightened concerns on the potential impacts of fugitive CH₄ emissions to the subsurface and atmosphere (Jackson et al., 2014). Methane (the primary component of natural gas) is a greenhouse gas of concern due to its global warming potential that is 86 times greater than that of CO₂ over 20 yr and 25 times greater over 100 yr (Myhre et al., 2013). Methane can be released to the atmosphere through surface casing vent flows and/or to the subsurface and atmosphere from stray gas migration (GM). Both pathways are a result of imperfectly sealed oil and gas wells. In the case of GM, gas enters the subsurface along a leaky well bore and, driven by its buoyancy, migrates upward toward overlying freshwater aquifers and the vadose zone (Davies et al., 2014; Dusseault and Jackson, 2014). Methane migration as a result of well integrity failure is well documented in the oil and gas industry and, aside from surface casing vent flows, continues to pose the most likely pathway for gas to reach the ground surface (Davies et al., 2014; Dusseault and Jackson, 2014; Dusseault et al., 2000; Erno and Schmitz, 1996; Hammond, 2015; Harrison, 1983, 1985; Watson and Bachu, 2009). In Alberta, Canada, a recent report estimated that 0.73% of 3276 wells had compromised well casings resulting in GM (Bachu, 2017). In the United Kingdom, elevated CH₄ soil gas concentrations at 30% of 102 abandoned and decommissioned oil and gas wells were attributed to GM (Boothroyd et al., 2016). Various studies have also reported the occurrence of GM from faulty well casings via the detection of dissolved CH₄ in aquifers (Darragh et al., 2014; Jackson et al., 2013; Osborn et al., 2011) and CH₄ emissions to the atmosphere (Allen et al., 2013; Caulton et al., 2014; Johnson et al., 2017; Kang et al., 2016; Lan et al., 2015).

Although these studies have traced the origin of fugitive CH₄ to leakage from compromised well casings, there is a need to better understand the pathways and mechanisms of fugitive CH₄ migration at a scale that is appropriate to a single extraction well and for a leakage event of known magnitude and duration (Council of Canadian Academies, 2014).

Research on gas transport mechanisms in porous media (including CH₄ GM) has shown that small-scale heterogeneities may result in lateral and discontinuous gas transport (Gorody, 2012; Mumford et al., 2010; Steelman et al., 2017; Tomlinson et al., 2003). Methane release from the saturated zone into the vadose zone may occur if buoyancy forces are great enough to overcome capillary forces (Gorody, 2012). In addition, gas release to the vadose zone may be influenced by barometric pressure and water table fluctuations (Baird et al., 2004; Strack and Waddington, 2008; Strack et al., 2006; Zhang et al., 2012). Vertical GM can result in surface effluxes of CH₄ and CO₂, as previously shown at petroleum hydrocarbon spill sites (Sihota et al., 2013). In the presence of oxygen (O₂), CH₄ can undergo aerobic oxidation driven by methanotrophs to produce CO₂ (Bogner et al., 1997). Significant CH₄ and CO₂ effluxes due to GM from imperfectly sealed oil and gas wells pose a global environmental concern for greenhouse gas emissions and a local risk of explosion if CH₄ concentrations in soil gas exceed 5% (v/v). Various studies have used numerical modeling to characterize the fate and transport of CH₄ gas due to well bore leakage in the saturated zone (Nowamooz et al., 2015; Rice et al., 2018; Roy et al., 2016). However, in the context of fugitive GM, no studies to our knowledge have conducted numerical modeling of the transport and reaction mechanisms affecting the fate of CH₄ in the vadose zone. Numerical models suitable for simulation of the fate of CH₄ in the vadose zone are available. For example, Sihota and Mayer (2012) and Molins et al. (2008) used reactive transport modeling (RTM) to characterize gas transport and reaction processes at a site contaminated with petroleum hydrocarbons and in landfill covers, respectively. Without a comprehensive understanding of the migration and fate of fugitive CH₄, it remains difficult to delineate and quantify emissions to the atmosphere related to GM originating from oil and gas wells.

Recently, a controlled subsurface natural gas release experiment was conducted at the Canadian Forces Base (CFB) Borden, Alliston, Ontario, Canada. Over 72 d, 51 m³ of natural gas (>93% CH₄) was injected at depths of 4.5 and 9 m in a shallow, unconfined sand aquifer (Cahill et al., 2017, 2018; Steelman et al., 2017). Below the water table, free-phase CH₄ migration was influenced by small-scale heterogeneities and resulted in extensive lateral GM downgradient of the injection location (Cahill et al., 2018). Episodic releases of free-phase gas were measured at the ground surface as CH₄ effluxes. Measurements over 12 d of the 72-d experiment demonstrated both spatial and temporal variability of gas effluxes, despite the proximity of measurement locations to the injection point and a continuous injection rate (Cahill et al., 2017). Cahill et al. (2017) also suggested that a substantial

portion of the injected CH₄ was lost to oxidation in the vadose zone, whereas minimal oxidation occurred in the saturated zone during the period of gas injection. Although Cahill et al. (2017) provided an overview of the study results, including vadose zone responses, a detailed analysis of CH₄ GM mechanisms and fate from the vadose zone to the ground surface for the entire duration of the experiment was not provided.

The current contribution focuses on the interpretation of the complete data set, including spatial and temporal effluxes for CH₄ and CO₂, vadose zone soil gas concentrations, and stable carbon isotope ratios measured over the 89-d experiment encompassing baseline monitoring, all injection phases, and the recovery period after injection. Results are supplemented with quantitative and process-based RTM to identify the dominant transport and reaction mechanisms affecting CH₄ for a range of CH₄ effluxes. The overall goal of this study is to contribute to a better understanding of the spatial distribution, temporal evolution, migration, and fate of CH₄ in the vadose zone and the potential for fugitive gas emissions to the atmosphere.

Specific objectives of this study were (i) to evaluate the magnitude and spatiotemporal distribution of surficial CH₄ and CO₂ effluxes as a function of gas injection rates, (ii) to assess the evolution of GM processes and CH₄ oxidation in the vadose zone, (iii) to estimate the fraction of injected CH₄ lost from the saturated zone and emitted to the atmosphere as CH₄, and (iv) to discuss the implications for monitoring and detecting fugitive CH₄.

Materials and Methods

Site Description and Natural Gas Injection

A controlled natural gas release experiment was conducted at the CFB Borden, Alliston, Ontario, Canada. The shallow, unconfined glacio-lacustrine sand aquifer at the site has been well characterized through various studies (Sudicky and Illman, 2011), allowing for a focused analysis on the fate and transport of fugitive CH₄. The aquifer extends 7 to 9 m below the ground surface and is underlain by a silt aquitard. The aquifer contains horizontal discontinuous lenses of medium-grained, fine-grained, and silty fine-grained sand with infrequent silt, silty-clay, and coarse sand layers (Sudicky and Illman, 2011). The water table is located 1 m (±0.5 m) below the ground surface, providing an opportunity to study GM representative for sites with a shallow water table. Such conditions occur, for example, at some oil and gas plays in northeastern British Columbia, Canada (Ferbey et al., 2008).

Over 72 d, 51 m³ (at 0.1013 MPa and 15°C) of natural gas (93.8% CH₄, 3.8% C₂H₆, 0.3% C₃H₈, ~0.1% C₄₊, 1.1% N₂, 0.8% CO₂, 0.05% O₂) was injected using inclined sparging wells at depths of 4.5 and 9 m below ground surface (Fig. 1). The injection wells were installed at a 45° angle to minimize vertical CH₄ migration along the well. Wells were installed using a Geoprobe (model 7822DT) direct push system in a vertical plane perpendicular to groundwater flow. Natural gas was injected from gas canisters

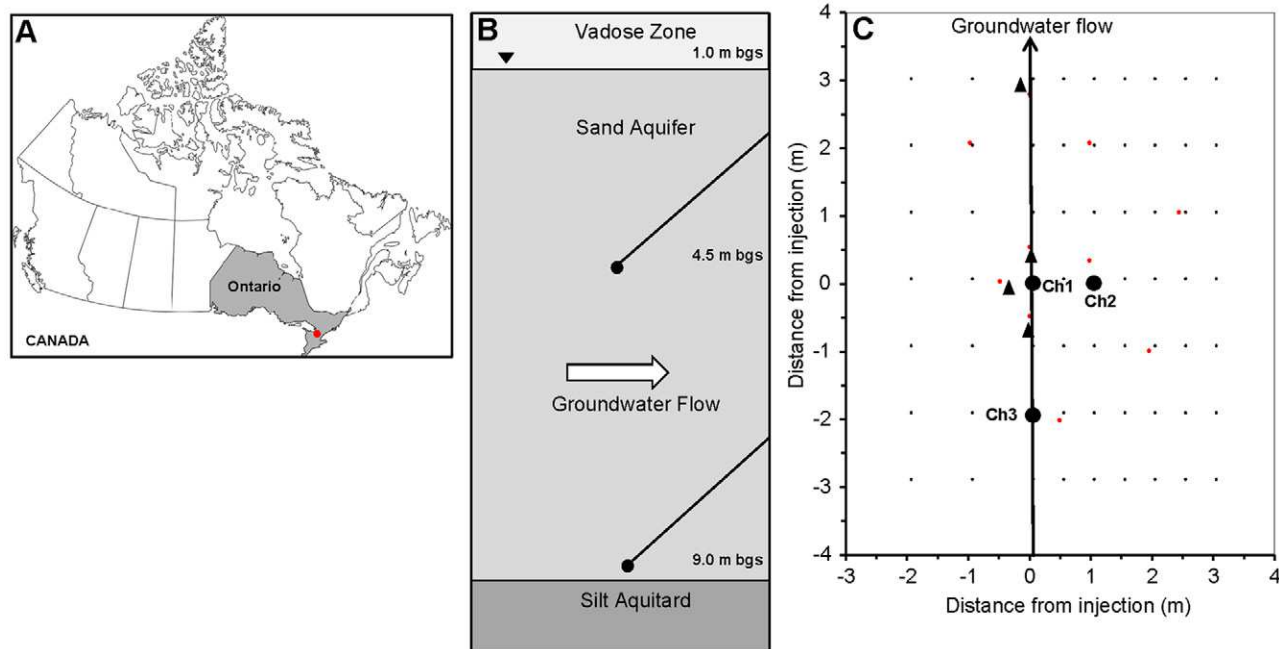


Fig. 1. (A) Map of Canada with the location of the Canadian Forces Base Borden in Ontario marked by a red dot. (B) Borden aquifer hydrological setting with a thin vadose zone and a relatively homogenous sand aquifer underlain by a silt aquitard. Injection points are labeled at their respective depths below ground surface (bgs). (C) Monitoring network. Small black dots represent survey efflux measurement locations; large black dots indicate long-term chambers Ch1, Ch2, and Ch3 as labeled; triangles indicate sensor locations; red dots represent soil gas monitoring wells at depths of 10, 30, and 50 cm.

connected via polyethylene tubing to the injection ports. Injection rates were adjusted incrementally and controlled by in-line electronic mass flow controllers (Red-y smart GSC-C9SA-BB26) with the associated software (Get Red-y, Vögtlin Instruments AG). When the injection phases were completed (Day 72), the wells were sealed with no-return valves to prevent flow-back of gas.

The varying injection rates of the experiment are categorized into five phases, including the recovery period after injection (Table 1). The injection rate increased from Phase 1 to Phase 4; however, the shallow injection well (4.5 m) was turned off in Phase 3. Surface casing vent flows indicate leakage within a well and can be used as a proxy for the occurrence of GM. Gas injection rates were based on reported surface casing vent flows from Alberta and British Columbia, Canada (Nowamooz et al., 2015), assuming that leaky wells could lead to GM of similar magnitude. Vadose zone and surficial monitoring commenced 2 d prior to and continued until 15 d after the end of injection, corresponding to a period of investigation of 89 d.

Soil Gas Effluxes

Three long-term dynamic closed chambers (LI-8100-104, LI-COR Inc.) were used in combination with a multiplexer (LI-8150, LI-COR Inc.) and a CO₂ infra-red gas analyzer (LI-8100, LI-COR Inc.) to monitor water vapor and CO₂ effluxes throughout the experiment (Fig. 1). Coupled with these instruments, water vapor, CH₄, and CO₂ effluxes were measured with an extended-range (0.01–100,000 ppm) ultraportable greenhouse gas analyzer (Los Gatos Research Inc.). Measurements were conducted approximately

every 15 min at each chamber. Periodically, the long-term chambers were disconnected to complete survey measurements (over ~2 to 6 h) on a monitoring grid including up to 63 locations (Fig. 1). Measurements were completed with a survey chamber (LI-8100-103, LI-COR Inc.) connected to the infrared gas analyzer and the ultraportable greenhouse gas analyzer. The instrumental setup for the flux measurements followed the approach by Sihota et al. (2013).

The survey and long-term chambers were placed on preinstalled polyvinyl chloride collars (20 cm i.d.) covering an area of 317.8 cm². The collars were inserted at least 4 cm into the soil 1 wk prior to commencing the gas injection to allow soil gas effluxes to equilibrate (Law et al., 2001). Long-term chambers were colocated with in-soil volumetric water content (VWC), electrical conductivity, temperature sensors, and soil gas sampling ports. The purpose of the long-term chambers was to monitor the temporal evolution of effluxes at selected locations close to the injection well. The survey measurements were completed to periodically monitor the spatial distribution of effluxes

Table 1. Experimental phases for natural gas injection and recovery periods.

Phase	Duration	Shallow	Deep	Total rate
		injection rate	injection rate	
	d	L min ⁻¹		L d ⁻¹
I	28	0.06	0.06	172.8
II	40	0.35	0.35	1008
III	2	0	0.35	504
IV	2	1.5	1.5	4320
V	15	0	0	0

(Fig. 1). In addition, effluxes at one background location (outside the monitoring area shown in Fig. 1 but with similar vegetation) were measured with every survey campaign.

Soil gas effluxes (F , in $\mu\text{mol m}^{-2} \text{s}^{-1}$ or $\text{g m}^{-2} \text{d}^{-1}$) were calculated using well-established methods based on measured concentration changes in the chamber over the specified time interval ($\partial C/\partial t$) and the measured water vapor content (W), pressure (P), temperature (T), system volume (V), and measurement area (S) (LI-COR, 2015):

$$F = \frac{10VP(1-W/1000)}{RS(T+273.15)} \frac{\partial C}{\partial t} \quad [1]$$

where F is the soil gas efflux rate ($\mu\text{mol m}^{-2} \text{s}^{-1}$); P is the initial pressure (kPa); T is the initial air temperature ($^{\circ}\text{C}$); W is the initial water vapor model fraction (mmol mol^{-1}); V is the total system volume including chamber, analyzers, tubing, and soil collar (cm^3); R is the ideal gas constant ($8.314 \text{ Pa m}^3 \text{ K}^{-1} \text{ mol}^{-1}$); S is the soil surface area underneath the soil collar (cm^2); and $\partial C/\partial t$ is the initial rate of change of the water-corrected CO_2 or CH_4 mole fraction during measurement period ($\mu\text{mol mol}^{-1} \text{s}^{-1}$).

The chamber measurements were conducted for a period of 2.5 min. Observed linear concentration increases with durations ranging from 45 to 80 s were used to calculate the effluxes. Previous work has demonstrated that a linear approximation can be used effectively to compute effluxes for measurement durations in this range (Alm et al., 2007; Heijmans et al., 2004). Compared with an exponential regression, a linear approximation tends to provide a more conservative estimate of the efflux and thus reduces the risk of overestimation (Forbrich et al., 2010; Pihlatie et al., 2013). Average, minimum, and maximum CH_4 and CO_2 effluxes were calculated for each injection phase, excluding the 5-d power outage on Day 39 when no data were collected.

Soil Gas Sampling

Soil gas samples were collected from monitoring wells that were installed at 10 selected locations at depths of 10, 30, and 50 cm (Fig. 1). The monitoring wells consisted of 1/8-in gas impermeable polyethylene tubing with a mesh screen attached to the bottom and a gas-tight fitting and septa at the top. Three line volumes were purged using gas-tight syringes (Valco Instruments Co.). Samples were collected and stored in pre-evacuated 12-mL vials (Labco Ltd.). Gas composition analyses (CH_4 , CO_2 , N_2 , O_2 , and Ar) were completed at the University of British Columbia on a Varian MicroGC CP-4900 dual-channel gas chromatograph equipped with a MolSieve 5a column (for O_2 , N_2 and Ar), a PoraPlot Q column (for CH_4 and CO_2), and micro-machined thermal conductivity detectors. The method of analysis on the GC followed Amos et al. (2005) and Sihota et al. (2011). Stable carbon isotope ratios ($^{13}\text{C}/^{12}\text{C}$) of CH_4 and CO_2 were measured in the Isotope Science Laboratory at the University of Calgary (Alberta, Canada). Analyses were completed on a ThermoFisher MAT 253 isotope ratio mass spectrometer coupled to Trace

GC Ultra + GC Isolink (ThermoFisher) (Humez et al., 2016). Results are reported in the internationally accepted delta ($\delta^{13}\text{C}$) notation (in ‰) relative to Vienna PeeDee Belemnite (VPDB) with a precision better than ± 0.5 and $\pm 0.3\%$ for $\delta^{13}\text{C}$ values of CH_4 and CO_2 , respectively.

Volumetric Water Content and Barometric Pressure

A datalogger (CR-1000, Campbell Scientific) was used to collect data from in-soil sensors for VWC, electrical conductivity, and temperature (CS650, Campbell Scientific). Sensors were placed 50 cm below the ground surface at four selected locations next to gas sampling ports and long-term chambers (Fig. 1). Barometric pressure was continuously recorded with a pressure transducer installed at the field site (Baro-Diver, vanEssen Instruments).

Mass Balance Calculations

Mass balance calculations were conducted using long-term and survey efflux data to estimate daily and cumulative CH_4 mass losses to the atmosphere. A detailed description of the methodology of the mass balance calculation can be found in the Supplemental Material.

Reactive Transport Modeling

The MIN3P-DUSTY RTM (Molins and Mayer, 2007) was used to quantitatively assess the subsurface fate of CH_4 . MIN3P-DUSTY accounts for geochemical reactions in the vadose zone, multicomponent solute transport, and advective-diffusive multicomponent gas transport. Gas diffusion is described by the Dusty Gas Model (Mason and Malinauskas, 1983; Sihota and Mayer, 2012) with species-dependent binary diffusion coefficients. Gas phase tortuosity is described with the Millington (1959) formulation (Sihota and Mayer, 2012). MIN3P-DUSTY has previously been used to simulate transport and reactions processes involving CH_4 at a hydrocarbon-contaminated site (Molins et al., 2010; Sihota and Mayer, 2012) and in landfill cover soils (Molins et al., 2008), confirming that the code is well suited for the process-based assessment of vadose zone CH_4 fate and transport in the current experiment.

Two simulations were completed targeting high and low CH_4 efflux conditions constrained by observations at Chamber 2 and the associated multilevel soil gas sampling well. Each simulation was completed using a one-dimensional domain describing a 70-cm soil column to represent the vertical extent of the vadose zone at the CFB Borden field site. The physical properties of the soil were selected based on literature values from previous experiments conducted at the site (Table 2). Gas concentrations at the upper boundary were fixed at atmospheric levels. Binary free-phase gas diffusion coefficients and viscosities were adopted from Sihota and Mayer (2012).

Reactive GM through the vadose zone was simulated for the low- and high-flow-rate regimes by applying a specified CH_4 influx at the base of the soil column, corresponding to the

observed total gas efflux ($\text{CO}_2 + \text{CH}_4$) for the relevant flow rate regime. The total influx introduced for the low-flux simulation was $6.7 \mu\text{mol m}^{-2} \text{s}^{-1}$ ($9.3 \text{ g CH}_4 \text{ m}^{-2} \text{ d}^{-1}$) and $113.9 \mu\text{mol m}^{-2} \text{s}^{-1}$ ($157.8 \text{ g CH}_4 \text{ m}^{-2} \text{ d}^{-1}$) for the high-flux regime. The gas introduced was assumed to have the same carbon isotope ratio as the injected CH_4 ($\delta^{13}\text{C}\text{-CH}_4 -42\%$). The $\delta^{13}\text{C}$ values for CO_2 in the injected gas (-10%) and produced by root respiration (-22%) were defined to represent values found in thermogenic shale gas (Dai et al., 2017; Golding et al., 2013) and in the organic horizon of soils (e.g., Bird and Pousai, 1997), respectively. The aerobic oxidation of CH_4 , including carbon isotope fractionation, was simulated following the approach of Sihota and Mayer (2012) (Table 3). A kinetic fractionation model was used to account for the preferred oxidation of $^{12}\text{C}\text{-CH}_4$ leading to the enrichment of $^{12}\text{C}\text{-CO}_2$ in soil gas (Sihota and Mayer, 2012). Reaction rates for CH_4 oxidation for high- and low-flux events were calibrated to reproduce field observations (Table 3). Following Sihota and Mayer (2012), it was assumed that close to 50% of the carbon oxidized during the CH_4 degradation process was sequestered in biomass (Table 3). Root respiration with its own characteristic carbon isotope signature (-22%) was also considered to contribute to CO_2 production in the upper 20 cm of the vadose zone. Calibrated reaction rates for root respiration were similar to those reported by Sihota and Mayer (2012) and Trumbore (2000) (Table 3).

The model was constrained by using data from high- and low-flux events from one vertical well, including data on VWCs, soil gas concentrations (CH_4 , CO_2 , N_2 , and O_2), stable carbon isotope ratios of CH_4 and CO_2 , and CH_4 and CO_2 effluxes. Due to the limited availability of vadose zone molecular and isotopic gas data, simulations were completed to represent steady-state conditions for the respective flow rate regimes. Recharge was set at 300 mm yr^{-1} to obtain water contents ranging from 0.27 near the base of the domain to 0.15 near the surface, consistent with field observations.

Table 2. Soil parameters used for low and high flux model simulations.

Parameter	Value	Reference
Hydraulic conductivity, m s^{-1}	6.5×10^{-5}	Allen-King et al. (1998)
van Genuchten parameters		
α , m^{-1}	2.0	Sudicky et al. (2010)
n	1.9	
Residual saturation, $\text{m}^3 \text{H}_2\text{O m}^{-3}$ porous medium	0.06	Sudicky et al. (2010)
Porosity, $\text{m}^3 \text{void m}^{-3}$ porous medium	0.35	Sudicky et al. (2010)

Results and Discussion

Magnitude and Spatiotemporal Distribution of Effluxes as a Function of Gas Injection Rates

Baseline CH_4 effluxes were monitored for 2 d prior to initiating the gas injection and remained nondetectable during this time. Within 5 h of commencing the injection ($0.04 \text{ m}^3 \text{CH}_4$ injected), CH_4 effluxes were observed at the surface. Throughout Phase 1, average CH_4 effluxes remained relatively constant, with values of 2.4, 8.8, and $0.01 \mu\text{mol m}^{-2} \text{s}^{-1}$ (3.3 , 12.2 , and $0.01 \text{ g CH}_4 \text{ m}^{-2} \text{ d}^{-1}$) for Chambers 1, 2, and 3, respectively (Table 4; Fig. 2). As the injection rate increased in Phase 2, effluxes increased, with average CH_4 effluxes at Chambers 1, 2, and 3 reaching 10.1 , 64.3 , and $3.3 \mu\text{mol m}^{-2} \text{s}^{-1}$ (14.0 , 89.1 , and $4.6 \text{ g CH}_4 \text{ m}^{-2} \text{ d}^{-1}$), respectively. Effluxes continued to rise in response to the highest injection rate in Phase 4, reaching 33.9 , 98.5 , and $5.5 \mu\text{mol m}^{-2} \text{s}^{-1}$ (46.9 , 136.5 , and $7.6 \text{ g CH}_4 \text{ m}^{-2} \text{ d}^{-1}$) at Chambers 1, 2, and 3, respectively, within 4 h (Tables 1 and 4). Methane effluxes showed an equally rapid response when the injection system was turned off. In Phase 3, when the 4.5-m injection well was turned off, CH_4 effluxes declined drastically to 3.6 , 11.0 , and $1.1 \mu\text{mol m}^{-2} \text{s}^{-1}$ (5.0 , 15.2 , and $1.5 \text{ g CH}_4 \text{ m}^{-2} \text{ d}^{-1}$) at Chambers 1, 2, and 3, respectively, within 6 h (Table 4; Fig. 2). In Phase 5, when the experimental

Table 3. Reaction stoichiometry and rate constants for low and high CH_4 flux simulations.

Process	Stoichiometry rate expression (R)	Rate, Monod, and inhibition constants†
<u>Low CH_4 flux simulation</u>		
Root respiration	$\text{CH}_2\text{O} + \text{O}_2 \rightarrow \text{CO}_2 + \text{H}_2\text{O}$	$k_{\text{CH}_2\text{O}} = 1.7 \times 10^{-8} \text{ mol dm}^{-3} \text{ s}^{-1}$
Methane oxidation	$\text{CH}_4 + 1.515\text{O}_2 \rightarrow 0.515\text{CO}_2 + 1.1515\text{H}_2\text{O} + 0.485\text{CH}_2\text{O}(\text{biomass})$ $R = -k_{\text{CH}_4} [C_{\text{CH}_4} / (K_{\text{CH}_4}^S + C_{\text{CH}_4})] [C_{\text{O}_2} / (K_{\text{O}_2}^S + C_{\text{O}_2})]$	$k_{\text{CH}_4} = 1.5 \times 10^{-8} \text{ mol L}^{-1} \text{ H}_2\text{O s}^{-1}$ $K_{12\text{CH}_4}^S = 1.0 \times 10^{-5} \text{ mol L}^{-1} \text{ H}_2\text{O}$ $K_{13\text{CH}_4}^S = 8.1 \times 10^{-8} \text{ mol L}^{-1} \text{ H}_2\text{O}$ $K_{\text{O}_2}^S = 3.1 \times 10^{-6} \text{ mol L}^{-1} \text{ H}_2\text{O}$
<u>High CH_4 flux simulation</u>		
Root respiration	$\text{CH}_2\text{O} + \text{O}_2 \rightarrow \text{CO}_2 + \text{H}_2\text{O}$	$k_{\text{CH}_2\text{O}} = 2.0 \times 10^{-8} \text{ mol dm}^{-3} \text{ s}^{-1}$
Methane oxidation	$\text{CH}_4 + 1.515\text{O}_2 \rightarrow 0.515\text{CO}_2 + 1.1515\text{H}_2\text{O} + 0.485\text{CH}_2\text{O}(\text{biomass})$ $R = -k_{\text{CH}_4} [C_{\text{CH}_4} / (K_{\text{CH}_4}^S + C_{\text{CH}_4})] [C_{\text{O}_2} / (K_{\text{O}_2}^S + C_{\text{O}_2})]$	$k_{\text{CH}_4} = 8.5 \times 10^{-8} \text{ mol L}^{-1} \text{ H}_2\text{O s}^{-1}$ $K_{12\text{CH}_4}^S = 1.0 \times 10^{-5} \text{ mol L}^{-1} \text{ H}_2\text{O}$ $K_{13\text{CH}_4}^S = 8.1 \times 10^{-8} \text{ mol L}^{-1} \text{ H}_2\text{O}$ $K_{\text{O}_2}^S = 3.1 \times 10^{-6} \text{ mol L}^{-1} \text{ H}_2\text{O}$

† K_p^S , half-saturation constant for the i th species; k_p , rate constant for the i th species.

Table 4. Soil gas effluxes throughout the experiment from all three chambers. Averages were determined using all long-term efflux measurements excluding the time period of the power outage.

Chamber	Statistic	Soil gas efflux			
		Phase 1	Phase 2	Phase 3	Phase 4
$\mu\text{mol m}^{-2} \text{s}^{-1}$					
<u>CH₄ efflux</u>					
1	avg.	2.38	10.12	3.62	33.89
	min.	ND	0.02	ND	0.01
	max.	15.84	32.91	22.37	79.05
	SD	1.54	5.39	7.59	20.61
2	avg.	8.76	64.26	11.04	98.52
	min.	ND†	1.18	ND	ND
	max.	122.50	2679	78.20	394.8
	SD	15.19	178.94	25.83	123.40
3	avg.	0.01	3.26	1.12	5.54
	min.	ND	ND	0.64	0.03
	max.	0.36	10.16	3.20	19.14
	SD	0.05	1.68	0.65	7.94
<u>CO₂ efflux</u>					
1	avg.	7.49	18.05	14.43	21.16
	min.	1.13	1.30	1.02	8.02
	max.	28.92	52.67	25.09	40.05
	SD	1.54	5.39	7.59	20.61
2	avg.	11.19	42.69	28.02	31.18
	min.	1.15	2.49	1.09	4.10
	max.	46.11	1006	47.41	74.47
	SD	6.43	56.25	7.68	16.40
3	avg.	6.86	11.71	5.38	9.16
	min.	1.60	1.71	1.13	4.57
	max.	37.09	31.49	15.50	14.67
	SD	2.56	5.06	3.19	1.87

† Nondetectable.

injection was complete by Day 72, CH₄ effluxes dissipated to non-detectable within 14 h at Chamber 1, 26 h at Chamber 2, and 45 h at Chamber 3. These results demonstrate that CH₄ release rates at the ground surface dynamically and rapidly respond to changes in subsurface injection rates and that surface release rates are a function of injection depth, as evidenced by the rapid decline of surface emissions during Phase 3.

However, effluxes did not reach steady-state conditions during each phase but fluctuated by typically two orders of magnitude at individual measurement locations despite constant injection rates (Fig. 2; Table 4). Although the highest injection rate was applied during Phase 4, the maximum CH₄ efflux at Chamber 2 was measured in Phase 2 (2679 $\mu\text{mol m}^{-2} \text{s}^{-1}$ [3713 g CH₄ m⁻² d⁻¹]) (Table 4; Fig. 2). During these episodic efflux events, CH₄ effluxes rapidly increased and then decreased over a few hours. For example, on Day 26 of Phase 1, CH₄ effluxes at

Chamber 2 increased from 4.0 to 120.1 $\mu\text{mol m}^{-2} \text{s}^{-1}$ (5.5–166.4 g CH₄ m⁻² d⁻¹) over 9 h and then decreased back to 4.0 $\mu\text{mol m}^{-2} \text{s}^{-1}$ (5.5 g CH₄ m⁻² d⁻¹) over 16 h. Peak effluxes at Chambers 1 and 3 were often not temporally correlated with the highest emissions measured at Chamber 2 (Fig. 2).

These episodic emission events can likely be explained by the periodic release of stored gas from the saturated zone. The observed behavior is consistent with free gas accumulation in the saturated zone in response to the injection, which led to pressure build-up that allowed the entrapped gas to overcome capillary forces and develop continuous pathways toward the vadose zone. The low solubility of CH₄ gas (31 mg L⁻¹ at 298.15 K and 100 kPa) contributed to the accumulation of free-phase gas in the subsurface during active gas injection. Geophysical and dissolved gas data (Cahill et al., 2017, 2018; Steelman et al., 2017) provide additional evidence for the buildup of free-phase gas below the water table. When gas inflow ceased (Phase 3 and Phase 5), total gas pressure in the subsurface dissipated and thus effluxes to the surface rapidly declined (Fig. 2).

Periodic surficial gas releases have also been reported for in situ air sparging studies (Johnson et al., 1993; Selker et al., 2006). During in situ air sparging, pressure buildup from continuous inflow of compressed air allows the gas to overcome capillary forces and displace pore water. As sparging continues, injected gas migrates along the path of least resistance (McCray and Falta, 1996), ultimately finding a pathway through or around low-permeability layers until breakthrough at surface. Upon loss of injection pressure, surface effluxes tend to decline rapidly (Selker et al., 2006; Tomlinson et al., 2003). These observations are consistent with the CH₄ migration patterns seen in the present study.

Thus, the observed localized episodic CH₄ effluxes are indicative of hydrostratigraphic traps leading to accumulations and intermittent releases of over-pressurized gas. However, despite significant fluctuations within each of the phases (Fig. 2), the magnitude of average CH₄ emission rates correlated well with increasing injection rates (Table 4).

Generally, CO₂ effluxes also displayed strong temporal variations and increased from Phase 1 to Phase 2 (Fig. 2). Average background CO₂ effluxes ranged from 0.7 to 3.0 $\mu\text{mol m}^{-2} \text{s}^{-1}$ (2.7–11.4 g CO₂ m⁻² d⁻¹) across all three long-term chambers. Effluxes increased during Phase 1 to averages of 7.5, 11.1, and 6.9 $\mu\text{mol m}^{-2} \text{s}^{-1}$ (28.5, 42.2, and 26.2 g CO₂ m⁻² d⁻¹) at Chambers 1, 2, and 3, respectively. Effluxes continued to rise in Phase 2, with averages of 18.1, 42.7, and 11.7 $\mu\text{mol m}^{-2} \text{s}^{-1}$ (68.8, 162.4, and 44.5 g CO₂ m⁻² d⁻¹) at Chambers 1, 2, and 3, respectively (Table 4). Although the injected gas contained some CO₂, the strong temporal increase of CO₂ effluxes provides clear evidence for the occurrence of microbially mediated CH₄ oxidation. This observation is in stark contrast to what was observed in the saturated zone, where the isotopic signature of the injected CH₄ remained similar to the injected gas for >100 d after injection, suggesting limited CH₄ oxidation below the water table (Cahill et al., 2018). Effluxes declined in Phase 3, when the shallow injection

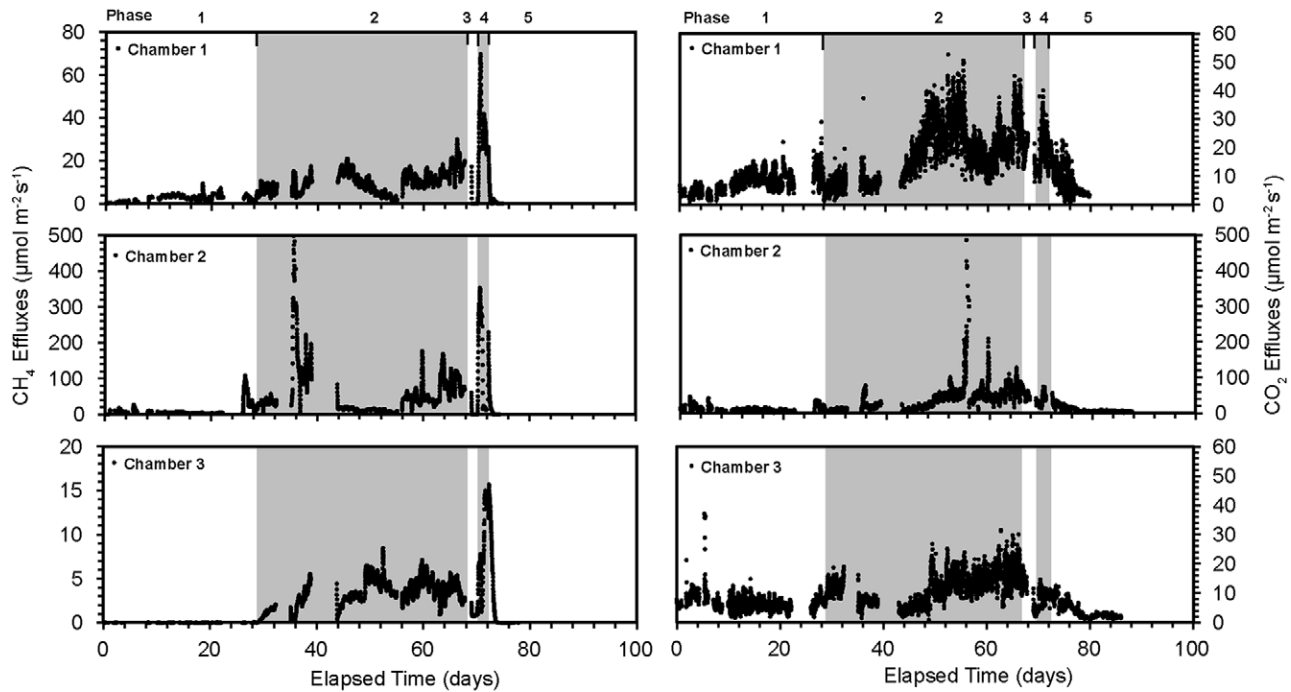


Fig. 2. Effluxes of CH_4 and CO_2 for long-term Chambers 1, 2, and 3 during injection Phases 1 to 4 and recovery Phase 5. Methane effluxes respond rapidly to changes in injection rates and are positively correlated; CO_2 effluxes generally also increase in response to the gas injection. Both CH_4 and CO_2 effluxes are characterized by strong temporal fluctuations independent of the injection rates.

well was turned off, but not as drastically as CH_4 effluxes; average CO_2 effluxes were 14.4, 28.0, and 5.4 $\mu\text{mol m}^{-2} \text{s}^{-1}$ (54.8, 106.5, and 20.5 $\text{g CO}_2 \text{m}^{-2} \text{d}^{-1}$) for Chambers 1, 2, and 3, respectively (Table 4; Fig. 2). The limited decline of CO_2 effluxes during Phase 3 suggests that CH_4 degradation was still occurring and that CH_4 was still released into the vadose zone, although at lower rates. During Phase 4, which had the highest injection rate, average CO_2 effluxes did not differ largely compared with those measured in Phase 2 and were only higher at Chamber 1 (by a factor of 1.2) (Table 4; Fig. 2). At Chambers 2 and 3, average CO_2 effluxes decreased in comparison to Phase 2, reaching only 70 to 80% of observed average Phase 2 effluxes (Table 4). The fact that CO_2 effluxes did not increase further or even declined during the highest injection rate suggests that CH_4 oxidation was inhibited by O_2 displacement from the vadose zone, which can be caused by substantial advective CH_4 effluxes (Molins et al., 2008). The longer persistence in CO_2 effluxes compared with CH_4 effluxes in Phase 5 suggests that residual CH_4 present in the vadose zone, or released from the saturated zone, continued to undergo oxidation (Fig. 2).

Results from survey measurements provide additional insight and demonstrate how the phased gas injection influenced the spatial distribution and magnitude of CH_4 and CO_2 effluxes. Results indicate greater lateral migration across the site in response to increasing injection rates. Throughout the experiment, CH_4 effluxes were relatively contained within a continuous hot spot in close proximity (within 2 m) to the injection location but were not directly located above the injectors (Fig. 3A). With time, and

as the injection rate increased, larger CH_4 effluxes and greater lateral migration were observed, with measurable effluxes up to 3 m from the injection location. Higher CH_4 effluxes were measured downgradient, as opposed to upgradient, of the injection point relative to the direction of groundwater flow, particularly with the highest injection rate in Phase 4 (Fig. 3A). The areal extent of CH_4 effluxes increased from 15 m^2 with maximum effluxes of 7.0 $\mu\text{mol m}^{-2} \text{s}^{-1}$ (9.7 $\text{g CH}_4 \text{m}^{-2} \text{d}^{-1}$) in Phase 1 to 25 m^2 with effluxes up to 623.1 $\mu\text{mol m}^{-2} \text{s}^{-1}$ (863.5 $\text{g CH}_4 \text{m}^{-2} \text{d}^{-1}$) in Phase 4. On the other hand, in Phase 3, CH_4 effluxes declined at all measurement locations and were highest upgradient of the injection location (10.1 $\mu\text{mol m}^{-2} \text{s}^{-1}$ [14.0 $\text{g CH}_4 \text{m}^{-2} \text{d}^{-1}$]) (Fig. 3A). A similar observation was made with the survey measurement CO_2 effluxes, which increased from Phase 1 to Phase 2, with a greater lateral reach of elevated emissions approaching an areal extent of 25 m^2 (Fig. 3B). During Phase 4, the greatest CO_2 efflux was measured with the survey chamber (71.5 $\mu\text{mol m}^{-2} \text{s}^{-1}$ [271.9 $\text{g CO}_2 \text{m}^{-2} \text{d}^{-1}$]) 1 m upgradient of the injection location (Fig. 3B).

The spatial distribution and evolution of surficial effluxes was supported by the observed soil gas concentrations. After the injection commenced, CH_4 concentrations within the vadose zone at a depth 50 cm had a similar spatial distribution to that of the corresponding surface effluxes (compare Fig. 3A and 4A). A CH_4 hot spot was observed in the vadose zone located adjacent to Chamber 2, 1 m offset from the injection location. As was observed for CH_4 effluxes, vadose zone CH_4 gas concentrations increased with greater injection rates and declined when

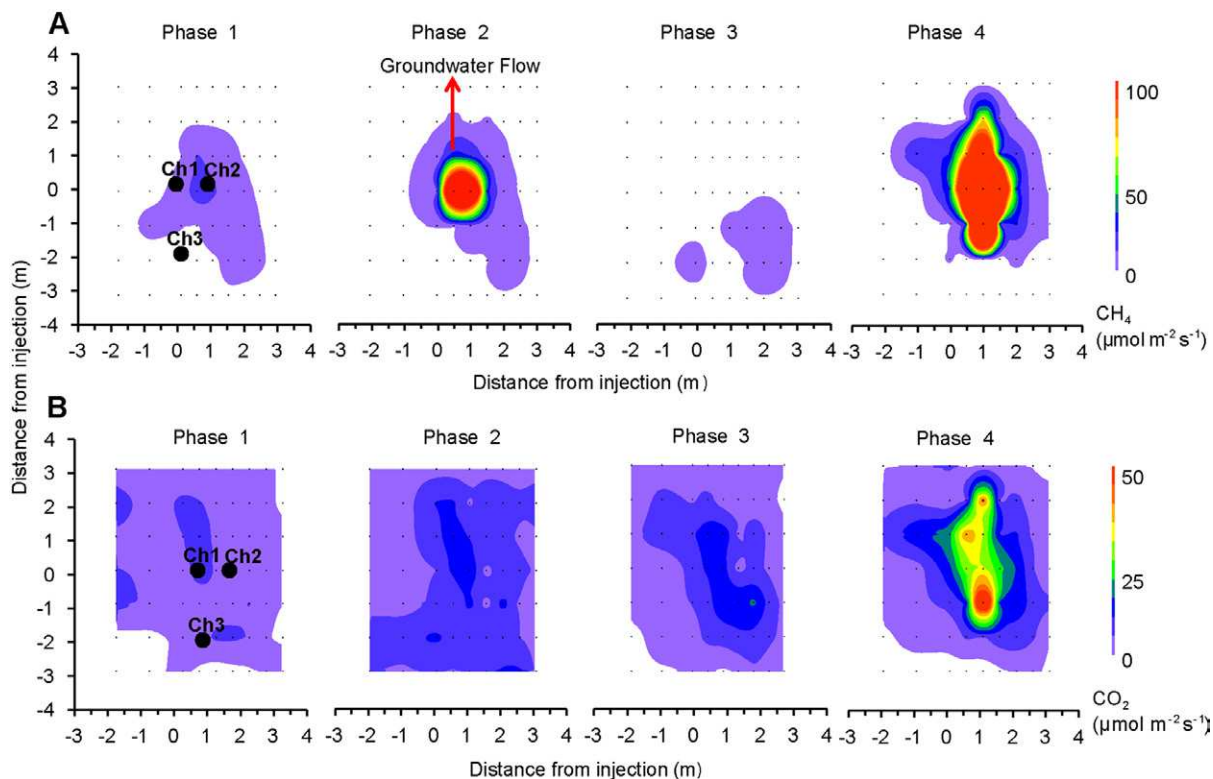


Fig. 3. Spatial distribution of (A) CH₄ effluxes and (B) CO₂ effluxes from Phases 1 to 4 taken with survey measurements on Day 27, 35, 70, and 72, respectively. Black points indicate survey measurement locations, and symbols denote the location of long-term chambers (Ch1, Ch2, and Ch3). The magnitude and spatial distribution of effluxes generally increased with greater injection rates.

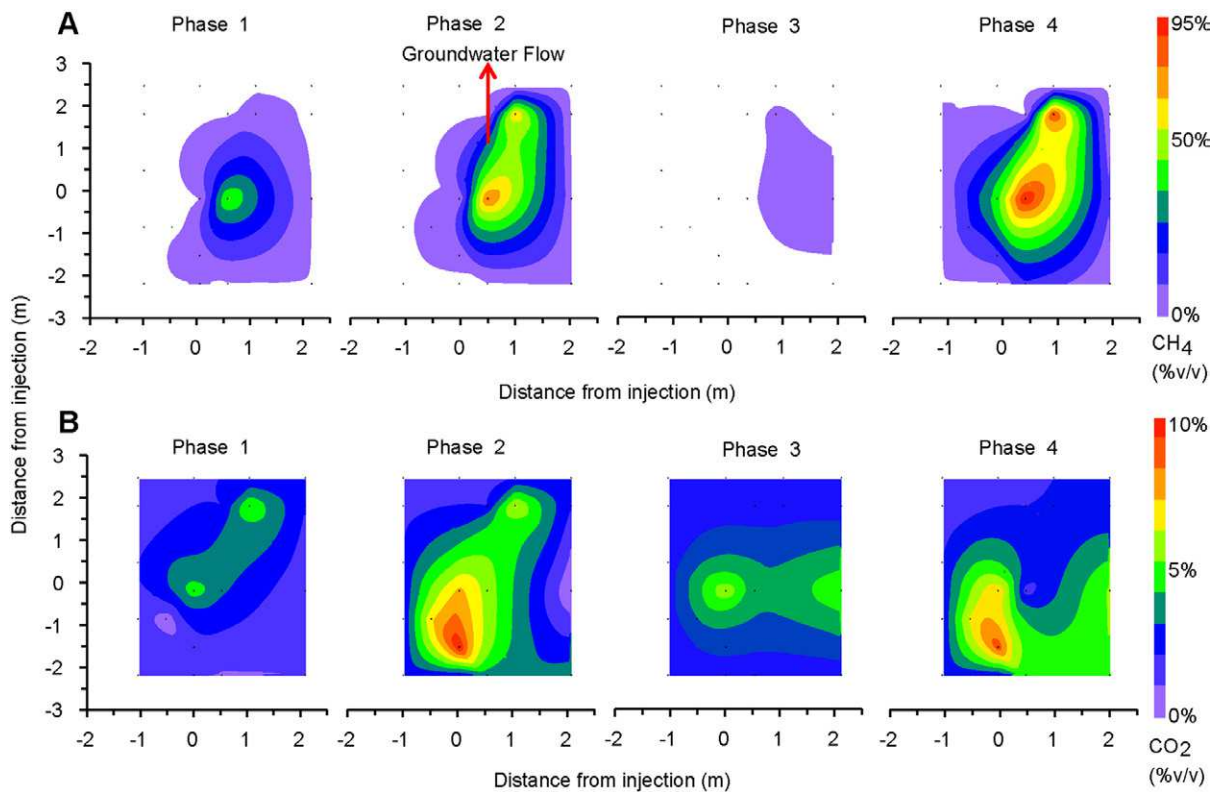


Fig. 4. Gas concentration (% v/v) at 50 cm depth from Phase 1, 2, 3, and 4 taken on Day 27, 35, 70, and 72, respectively, for (A) CH₄ and (B) CO₂. Black points indicate sampling locations for which samples were collected within an hour of each other over one sample round. Gas concentrations increased with greater injection rates.

the 4.5-m injector was turned off in Phase 3. During Phase 1, CH₄ concentrations reached 50% (v/v) within the hotspot and increased to >90% (v/v) during the highest injection rate (Phase 4). In Phase 3, CH₄ soil gas concentrations declined to <5% (v/v). Similar to the surficial effluxes, CH₄ soil gas concentrations increased preferentially in the direction of groundwater flow. In Phases 2 and 4, CH₄ concentrations >30% (v/v) were observed up to 2 m downgradient of the injection location (Fig. 4A). Concentrations of CO₂ soil gas at 50 cm depth also followed a similar spatial distribution to the effluxes, with higher concentrations along the center line and upgradient of the injection point relative to the groundwater flow direction (compare Fig. 3B and 4B). The spatial extent of the CO₂ soil gas plume grew during Phase 2 of the experiment, with concentrations up to 10% (v/v) observed up to 2 m away from the injection site. Concentrations of CO₂ within the CH₄ hotspot tended to be lower than those at the fringe of the hotspot. This was particularly observed during the highest injection rate when CO₂ was below 1% (v/v) at the CH₄ hotspot (Fig. 4B).

The fact that the highest CH₄ and CO₂ effluxes (at Chamber 2) were horizontally offset 1 m from the injection point further highlights that GM was affected by aquifer heterogeneities. The aquifer at the field site is known to consist of fine silt lenses that can result in preferential GM and lateral gas displacement (Tomlinson et al., 2003). The effects of soil heterogeneity on GM have also been reported by Delahaye and Pérez de Agreda (2002) and Esposito (2014) and in laboratory experiments (Chamindu Deepagoda et al., 2016). Increased CH₄ surface emissions and soil gas concentrations along the direction of groundwater flow (3 m downgradient) (Fig. 3A and 4A) suggest that free-phase CH₄ was “dragged” along with flowing groundwater and subsequently contributed to emissions. Over the duration of the experiment, CH₄ and CO₂

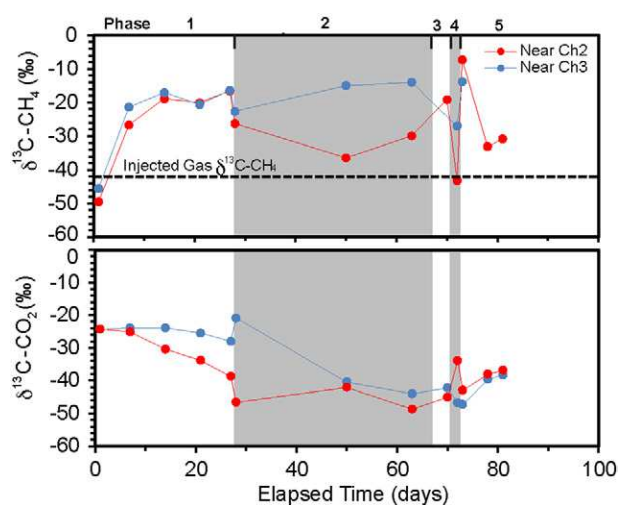


Fig. 5. Stable carbon isotopic composition (‰) at 50 cm depth measured over time near Chambers 2 and 3. The $\delta^{13}\text{C}-\text{CH}_4$ values increase beginning in Phase 1, whereas $\delta^{13}\text{C}-\text{CO}_2$ values decrease. Isotopic compositions are similar to the injected gas during the highest injection rate (Phase 4).

surface emissions and soil gas concentrations increased and extended 3 m downgradient of the injection location, confirming lateral gas displacement in the vadose zone (Fig. 3 and 4). Similar observations were made in the saturated zone where the highest injection rate (Phase 4) resulted in extensive dissolved CH₄ plumes at 2- and 6-m depths, reaching as far as 10 m from the injection location in the direction of groundwater flow (Cahill et al., 2018). Maxima both in terms of emissions and soil gas concentrations tended not to be collocated for CH₄ and CO₂, suggesting complex interactions between GM and CH₄ oxidation processes in the vadose zone.

Evolution of Gas Migration and Methane Oxidation Processes in the Vadose Zone

Stable carbon isotope values in CO₂ and CH₄ from a depth of 50 cm near Chambers 2 and 3 confirm the occurrence of CH₄ oxidation and indicate that oxidation began within the first 7 d of injection (Fig. 5). There was insufficient background CH₄ to determine its $\delta^{13}\text{C}$ value. The $\delta^{13}\text{C}$ value of the injected CH₄ was -42‰ and hence was markedly different from the carbon isotope ratios of biogenic CH₄. Background soil gas CO₂ had a $\delta^{13}\text{C}$ value of -24‰ . Trends over time indicate an increase for $\delta^{13}\text{C}-\text{CH}_4$ in soil gas to values around -20‰ , with $\delta^{13}\text{C}-\text{CO}_2$ values decreasing to below -40‰ near Chambers 2 and 3 (Fig. 5). Enrichment of ¹³C in CH₄ and ¹²C in CO₂ indicates microbial degradation of CH₄ due to the preferential utilization of CH₄ containing the light isotope (¹²C) to produce CO₂ (Whiticar and Faber, 1986). This was particularly noticeable toward the end of Phase 2 at Chamber 2 when $\delta^{13}\text{C}-\text{CO}_2$ values became more negative. During the same period, a rise in CO₂ effluxes and a decline in CH₄ effluxes were observed at Chambers 1 and 2 (Fig. 2), consistent with accelerating microbially mediated CH₄ oxidation.

Correlating the isotopic data for CH₄ and CO₂ with the magnitude of CH₄ effluxes reveals that lower CH₄ effluxes to the atmosphere ($0.01\text{--}10.0 \mu\text{mol m}^{-2} \text{s}^{-1}$ [$0.01\text{--}13.8 \text{g CH}_4 \text{m}^{-2} \text{d}^{-1}$])

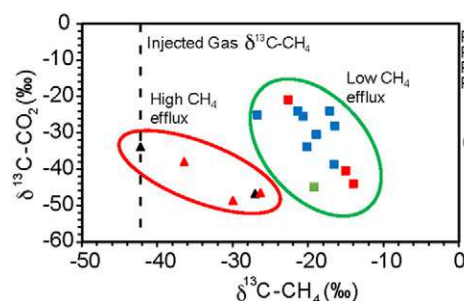


Fig. 6. Isotopic composition of soil gas samples collected at various locations at 50 cm depth throughout the experiment. Different CH₄ gas injection rates are indicated with respective colors for each phase. Methane effluxes measured at the surface prior to sampling are indicated by the shape, where squares represent effluxes between 0.01 and $10 \mu\text{mol m}^{-2} \text{s}^{-1}$ and triangles indicate effluxes $>10 \mu\text{mol m}^{-2} \text{s}^{-1}$. Advective gas migration is evident with higher CH₄ effluxes during Phase 2 and in Phase 4.

are synonymous with greater progression of aerobic CH₄ oxidation, whereas higher CH₄ effluxes show CH₄ signatures closer to the isotopic composition of the injected CH₄. However, samples from high-efflux events still show substantial enrichment of ¹²C-CO₂, indicating that CH₄ oxidation is occurring (Fig. 6). This observation implies that CH₄ oxidation capacity is limited and that under high-flux conditions only a relatively small fraction of CH₄ released into the vadose zone is oxidized prior to arrival at the ground surface.

Baseline soil gas concentrations measured 2 d prior to commencing injection showed that CH₄ concentrations were nondetectable, CO₂ ranged from 2 to 3% (v/v), O₂ ranged from 17 to 19% (v/v), and N₂ ranged from 78 to 79% (v/v) across all locations. From Phase 1 to Phase 2, N₂, CH₄, and CO₂ increased and O₂ decreased near Chambers 1 and 3 (Fig. 7). A rise in CO₂ concentrations supports increasing rates of CH₄ oxidation, which were most visible for gas samples collected near Chamber 3. The decline in partial pressures of CH₄ and O₂ due to CH₄ oxidation causes downward advective gas transport into the soil, leading to increased N₂ gas concentrations. Similar observations have been made at a crude oil spill site (Amos et al., 2005; Molins and Mayer, 2007; Revesz et al., 1995). Evidence for downward advection into the reaction zone is most visible during the early stage of Phase 2 (near Chamber 1) and throughout Phase 2 near Chamber 3 (Fig. 7). On the other hand, Amos et al. (2005) also showed that depletion of N₂ in the vadose zone is indicative of upward advective gas transport, here caused by the displacement of soil gas by the injected CH₄. Such conditions are clearly visible in most soil gas samples near Chamber 2, during the latter part of Phase

2 near Chamber 1, and at all sampling locations during the period with the highest injection rate (Phase 4) (Fig. 7).

Reactive transport modeling was used to further help delineate the governing transport processes and biogeochemical reactions. The model was constrained by data from Chamber 2 for a low-flux event that occurred on Day 28 (Phase 2) during the lowest injection rate and for a high-flux event that occurred on Day 72 during the highest injection rate (Phase 4). For both scenarios, model results were compared with the gas composition (% v/v) and stable C isotope ratios (¹³C/¹²C) of CO₂ and CH₄ from samples collected near Chamber 2 at depths of 10, 30, and 50 cm as well as with CH₄ and CO₂ effluxes measured at Chamber 2. Good agreement between simulated and observed results was obtained for both high- and low-flux conditions (Fig. 8 and 9).

In the high-flux simulation, CH₄ concentrations were elevated below a depth of 30 cm, whereas N₂ and O₂ were strongly depleted. Above 30 cm depth, the coexistence of O₂ and CH₄ provided conditions favorable for aerobic CH₄ oxidation, leading to maximum CO₂ concentrations at a depth of 20 cm (Fig. 8A). Values for δ¹³C-CH₄ remained relatively unchanged in comparison to the injected gas (-42‰), especially in the lower portion of the soil profile, where δ¹³C-CO₂ values were close to the background value (-24‰). In the upper portion of the soil profile, δ¹³C-CO₂ decreased to values of less than -40‰, whereas soil gas CH₄ became progressively enriched in ¹³C (Fig. 9A). These results indicate aerobic CH₄ oxidation in the upper 50 cm of the soil profile but with a limited impact on the isotopic composition of CH₄ due to its high abundance, consistent with data shown in Fig. 6. In addition, the simulations confirm that diffusive O₂ influxes were partially offset by advective O₂ effluxes and limited overall O₂ ingress and consequently CH₄ degradation (Fig. 10A). Model results also indicate that, for high-flux conditions, CH₄ and CO₂ fluxes were predominantly advective up to ~10 cm below the ground surface (Fig. 10A). In this region, a transition to a diffusion-dominated transport regime takes place and persists to the top of the soil column. The modeling supports the results and interpretations discussed above based on gas composition, efflux, and isotopic data.

Under low-flux conditions, CH₄ concentrations were lower than for high-flux conditions throughout most of the soil profile, particularly in the upper 30 cm. Conversely, O₂ concentrations penetrated deeper into the vadose zone, extending the region of active aerobic CH₄ oxidation to a greater depth and resulting in higher CO₂ concentrations at 20 cm (Fig. 8B). Values for δ¹³C-CH₄ increased, providing direct evidence for CH₄ oxidation (Fig. 9B). These results also suggest active aerobic oxidation of CH₄ in the upper 60 cm of the soil column. In the simulations, the carbon isotope ratios of CO₂ near the ground surface are affected by the process of root and soil respiration, explaining the return to less negative δ¹³C values (Fig. 9B). For low-flux conditions, advective CH₄ transport in the soil column is restricted to the lower part of the soil column and ends at a depth of ~45 cm, where fluxes become predominantly diffusive (Fig. 10B). The simulations also show that diffusive N₂ influxes were balanced by advective and nonequimolar (not shown) effluxes (Fig. 10B). Under low-flux

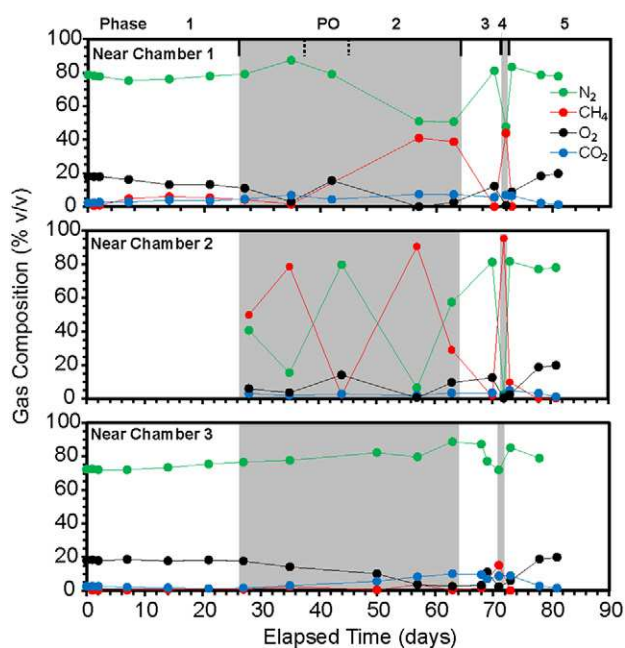


Fig. 7. Gas concentration (% v/v) over time measured at 50 cm depth near Chambers 1, 2, and 3. Methane concentrations increased with time, except during the power outage (PO) during Phase 2.

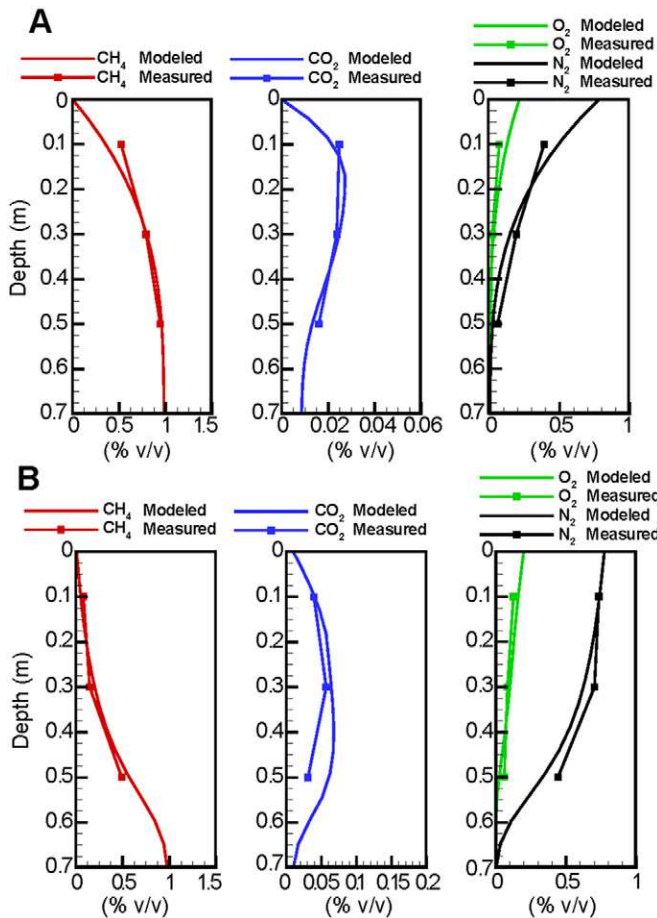


Fig. 8. Modeled and measured gas concentration profiles for (A) high and (B) low CH_4 flux conditions. Higher CH_4 concentrations with depleted N_2 concentrations are indicative of advective gas migration for the high-flux simulation. In contrast, lower CH_4 concentrations and larger N_2 concentrations are indicative of a more diffusion-dominated transport regime.

conditions, the results suggest that O_2 ingress was diffusion dominated with limited upward advection (Fig. 10B). These observations explain the greater depth of O_2 ingress under low-flux conditions in comparison to the high-flux case. Reactive transport modeling results further confirm that periods of low CH_4 effluxes allowed atmospheric O_2 to diffuse deeper into the soil column and promote greater and more complete oxidation of CH_4 .

Volumetric Water Content and Barometric Pressure

Volumetric water content in the vadose zone averaged $\sim 20\%$, with a few events where moisture contents temporarily increased after precipitation events. Barometric pressure fluctuated during the experiment between 97 and 101 kPa. Previous studies have indicated that these parameters can either enhance (Kim et al., 2012; Rey et al., 2017; Xu et al., 2014) or inhibit (Castro et al., 1995; Scheutz and Kjeldsen, 2004) GM to the surface and surface gas effluxes. Attempts to associate variations in moisture contents and barometric pressure to the episodic nature of the observed effluxes were

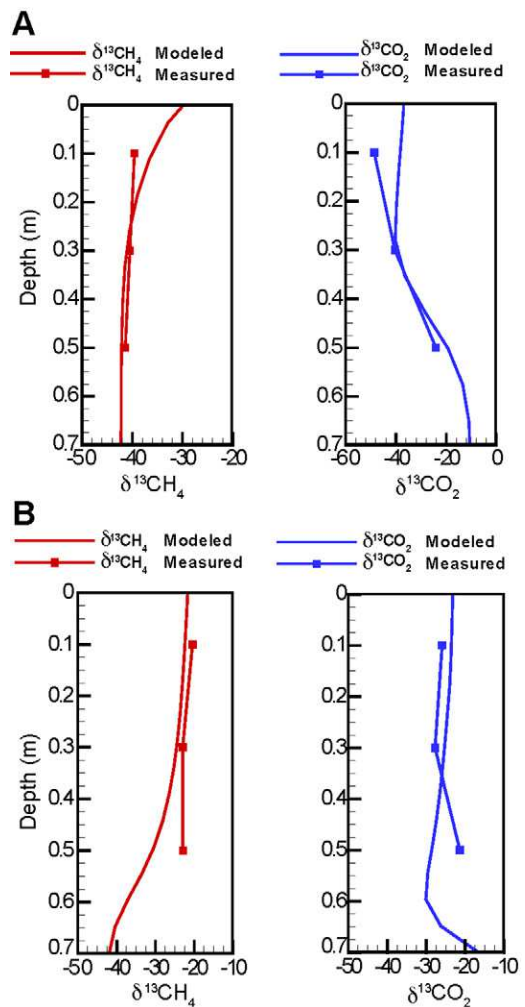


Fig. 9. Modeled and measured $\delta^{13}\text{C}$ values of CH_4 and CO_2 (in ‰) for (A) high and (B) low CH_4 flux conditions. High fluxes result in minimal change to $\delta^{13}\text{C}$ - CH_4 values in comparison to the injected gas. In contrast, the remaining CH_4 became enriched in ^{13}C during the low-flux simulation, indicating degradation.

not successful (not shown), suggesting that at this site subsurface processes controlled temporal evolution of the effluxes to a greater degree than VWC in the vadose zone and barometric pressure fluctuations. The limited thickness of the vadose zone and the relatively longer GM pathway through the saturated zone likely explain the lack of correlation of efflux data with atmospheric and vadose zone parameters.

Fraction of Injected Methane Lost from the Saturated Zone and Emitted to the Atmosphere as Methane

Mass balance calculations (see Supplemental Material for approach) indicate that, over 75 d of the experiment, $\sim 30\%$ of the injected CH_4 was emitted from the soil surface to the atmosphere as CH_4 effluxes (i.e., 12.2–15.3 m^3 compared with 51 m^3 injected). In Phase 1, a gradual increase in CH_4 effluxes was observed across all three long-term chambers until Day 26. Up to Day 26 $\sim 26\%$ of the total injected gas was emitted at the soil

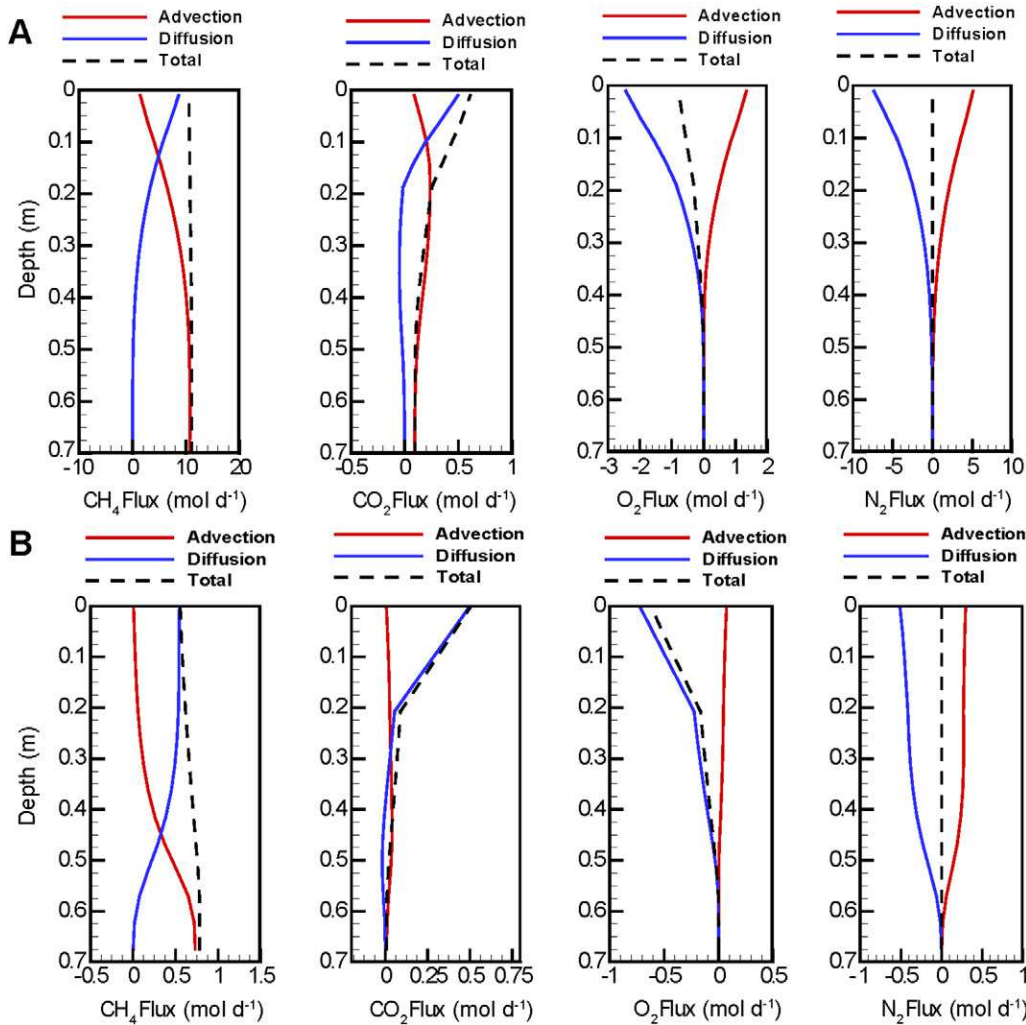


Fig. 10. Modeled CH_4 , CO_2 , O_2 , and N_2 fluxes for (A) high and (B) low CH_4 flux conditions. Advection is the dominant transport mechanism for CH_4 and CO_2 up to ~ 10 cm for high-flux conditions. For low-flux conditions, diffusion becomes dominant for CH_4 at 45 cm. Fluxes of CO_2 were dominated by the contributions of root respiration above a depth of 20 cm. Diffusive O_2 and N_2 influxes are counteracted by advective effluxes. For low-flux conditions, O_2 influxes are dominated by diffusion driven by root respiration and CH_4 oxidation.

surface to the atmosphere. However, on Day 26 alone, 72% of the gas injected on that day was emitted to the atmosphere. This likely represents the effect of gas entrapment in the saturated zone and pressure build-up prior to a sudden release. A similar effect was observed during Phase 2, with additional occurrences of episodic effluxes due to the higher injection rates and thus greater pressure forces for CH_4 gas to overcome capillary forces. Approximately 38% of the gas injected during Phase 2 was emitted from the soil surface to the atmosphere as CH_4 effluxes. Significant mass loss events can be identified when examining the cumulative mass release of CH_4 at the ground surface (Fig. 11). Mass loss on the day of episodic efflux events ranged from 38 to 261% of the gas injected that day. Methane loss greater than the injected mass on that day suggests that some of the injected CH_4 remained trapped below the surface until buoyancy forces were great enough to overcome capillary forces, resulting in a rapid cumulative release of gas. During Phase 3, only $\sim 15\%$ of the injected gas (from 9 m depth) was emitted from the soil surface to the atmosphere. However, the CH_4 effluxes measured could also be a result of the release of residual CH_4 gas injected earlier, not necessarily corresponding to emissions directly related to the active injection at 9 m depth. In Phase 4, 41% of the mass injected was lost to the atmosphere as CH_4 . The greater total CH_4 loss in each phase corresponds with

the increasing injection rates. However, the episodic high mass loss events within each phase also demonstrate that efflux at surface does not necessarily directly correspond to the magnitude of subsurface leakage.

Background CO_2 effluxes were too variable to reliably quantify the mass of injected CH_4 lost and emitted as CO_2 . However, rising CO_2 effluxes above background levels at all three chambers further confirm that some CH_4 was also lost to aerobic oxidation, yielding CO_2 as a product. In this context, the mass of dissolved CO_2 and other carbonate species retained in vadose zone pore water, expected in the presence of increased CO_2 partial gas pressures in soil gas, has been neglected, implying that the increase of CH_4 oxidation rates may be even more significant than inferred from the increasing CO_2 effluxes alone. Average CO_2 effluxes were greatest in Phase 2 (Table 4), suggesting that the microbial community had fully developed and that there was sufficient CH_4 and O_2 to drive methanotrophic oxidation of CH_4 . The cumulative mass of CO_2 emitted was greater than CH_4 emitted at Chambers 1 and 3, indicating that regions with lower CH_4 fluxes had relatively greater CH_4 loss to degradation (Fig. 11), consistent with the isotopic results (Fig. 6). Cumulative mass loss for CH_4 demonstrates that the episodic effluxes in Phase 2 and the high injection rate in Phase 4 resulted in significant,

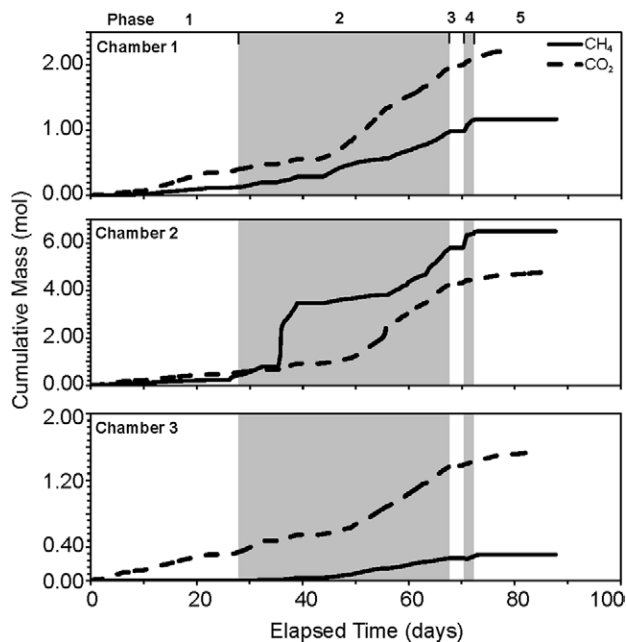


Fig. 11. Cumulative mass of CH₄ and CO₂ emitted over time for Chambers 1, 2, and 3. Episodic events during Phase 2 and in response to the high injection rate during Phase 4 resulted in significant CH₄ emissions. Greater CO₂ emissions at Chambers 1 and 3 are indicative of CH₄ oxidation.

yet short-lived, CH₄ emission events from the soil surface to the atmosphere (Fig. 11). In contrast, low fluxes allowed for a greater mass of CO₂ to be released through CH₄ oxidation. These trends are also supported by the RTM results, where high CH₄ fluxes resulted in limited CH₄ oxidation compared with low fluxes (Table 5).

In general, the method used to estimate the total CH₄ lost to the atmosphere (30%) does not account for losses due to oxidation and emissions as CO₂. It is likely that a significant portion of CH₄ was lost to oxidation, as indicated by the changes in stable carbon isotopes and the rise in CO₂ effluxes, particularly in Phase 2. Neglecting the emissions of CO₂ generated by CH₄ oxidation implies that the 30% estimate reported here may be conservative. However, the uncertainties associated with the mass balance estimate are substantial due to the small number of long-term chambers, the limited number of spatial surveys, and the assumption that measured CH₄ effluxes are representative of an area larger than that directly covered by the collar (see Methods in the Supplemental Material). The mass balance results must therefore be considered qualitative in nature.

Conceptual Model and Implications for Monitoring and Detecting Fugitive Methane

The experimental results demonstrate that subsurface gas leakage can result in spatially distributed and intermittent GM to the vadose zone, where both diffusion and advection contribute to CH₄ transport (Fig. 12). Advection is more likely to dominate under higher leakage rates (i.e., compare Phase 1

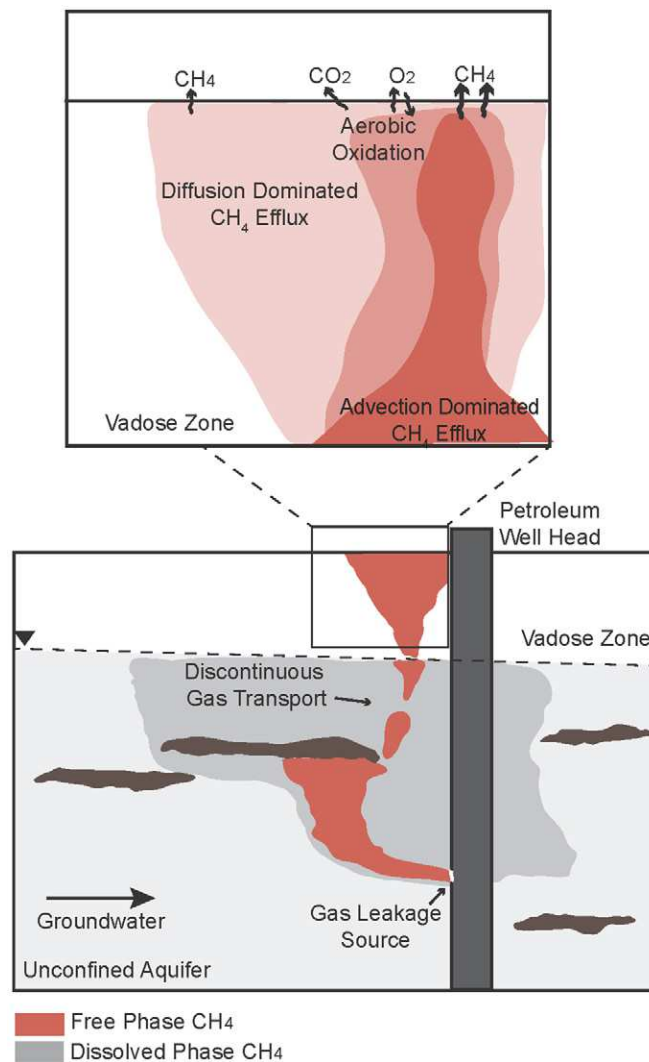


Fig. 12. Conceptual model of the fate of fugitive CH₄ in an unconfined aquifer and its overlying vadose zone. Free-phase CH₄ migrates vertically into the vadose zone along preferential pathways. At the base of the vadose zone, CH₄ migration is dominated by advective transport, resulting in higher CH₄ effluxes to the atmosphere above the source point. Methane undergoes aerobic oxidation as it migrates further from the source point, resulting in lower effluxes to the atmosphere dominated by diffusive transport.

with Phase 4) and where preferential pathways have formed (i.e., compare Chamber 2 with Chamber 3). Advection-dominated gas transport may lead to less complete CH₄ oxidation and result in larger CH₄ emissions at the surface. Diffusion-dominated transport tends to lead to more complete CH₄ oxidation, resulting in enhanced CO₂ emissions (Fig. 12). The episodic nature and complex spatial distribution of effluxes suggests that continuous long-term monitoring at multiple locations is needed to evaluate the occurrence and potential risks of fugitive CH₄ migration on oil and gas well pads.

The spatial distributions of CH₄ and CO₂ effluxes in this experiment were relatively contained in a 25-m² area (up to 3 m from the injection point) and increased with greater injection rates. However, the extent of lateral GM did not reach as far as the

Table 5. Mass balance results for low and high CH₄ flux simulations.

Parameter	Low flux		High flux	
	CH ₄	CO ₂	CH ₄	CO ₂
	————— μmol m ⁻² s ⁻¹ —————			
	<u>Measured</u>			
Efflux	2.43	7.41	106.94	6.83
	<u>Modeled</u>			
C source from injection and root respiration	6.71	3.36	113.89	4.05
C loss to gas phase	-4.86	-4.28	-107.75	-7.06
C source or loss from oxidation	-1.74	0.93	-6.13	3.01
Diffusive efflux	4.86	4.28	94.44	6.13
Advective efflux	0.00	0.00	13.19	0.91
C loss to storage gas phase	0.00	0.00	0.00	0.00

groundwater CH₄ plume in the saturated zone (3 vs. 10 m down-gradient of the injection location in the direction of groundwater flow) (Cahill et al., 2018; Steelman et al., 2017), suggesting that near-surface measurements may not capture the spatial extent and impact of fugitive gas releases on freshwater aquifers. This study demonstrated that subtle heterogeneities can have a significant impact on GM. It can be expected that greater lateral GM would occur in more heterogeneous media and for natural gas releases at greater depths. In addition, the vadose zone at this site was relatively thin (<1 m); in a deeper vadose zone, larger vertical distances to the ground surface could result in greater residence times for CH₄ gas. This could lead to a delayed response in effluxes at the surface, more lateral spreading, and greater CH₄ oxidation if O₂ can be supplied to depth.

Conclusions

Monitoring of a controlled natural gas release into a shallow unconfined aquifer provided the opportunity to evaluate the pathways and mechanisms of vadose zone GM and surface emissions. Results demonstrate that surficial CH₄ and CO₂ effluxes were strongly influenced by the rate of gas release into the aquifer and subsurface heterogeneity. Higher injection rates led to greater average CH₄ effluxes and lateral migration. As the injection rate increased, CH₄ migrated 3 m from the injection location and affected an area approaching 25 m². Despite continuous injection rates, effluxes were episodic in nature and varied in magnitude over time (e.g., CH₄ effluxes ranged from 1.2 to 2679 μmol m⁻² s⁻¹ [1.7–3713 g CH₄ m⁻² d⁻¹] at Chamber 2 in Phase 2). Temporal and spatial monitoring and RTM demonstrated that high CH₄ effluxes were governed by advective GM (Fig. 12). In contrast, low CH₄ efflux conditions were dominated by diffusive GM allowing for greater O₂ ingress and more complete CH₄ oxidation (Fig. 12). The increasing CO₂ effluxes and the change of carbon isotope ratios of CH₄ and CO₂ indicated that there was a strong propensity for CH₄ oxidation

in the vadose zone. This observation suggests that significant amounts of the injected CH₄ were lost to oxidation and emitted to the atmosphere as CO₂. The mass loss to the atmosphere is likely greater than what has been accounted for solely based on CH₄ effluxes (~30%). Our results demonstrate that, even in a relatively homogenous aquifer, subtle heterogeneities can lead to preferential pathways that influence the spatial and temporal distribution of CH₄ and CO₂ effluxes at the ground surface. Effluxes were found to be episodic and resulted in large, yet short-lived emissions of CH₄. In addition, localized hot spots led to subsurface CH₄ concentrations that reached high concentrations above the lower explosive limit (5% v/v) and in some cases exceeded 90% (v/v) CH₄ close to the ground surface.

These results allowed us to develop a conceptual model of fugitive CH₄ migration from the vadose to the ground surface (Fig. 12). Although recent research has focused on fugitive CH₄ impacts in the saturated zone and atmosphere, few studies have quantified and assessed migration from the saturated zone to the ground surface. Our conceptual model will help to inform monitoring of fugitive gas from oil and gas wells. The results demonstrate the need for subsurface characterization followed by continuous and spatially discrete monitoring from the aquifer to the ground surface to detect and quantify fugitive GM.

Acknowledgments

This work was supported by the Natural Sciences and Engineering Research Council of Canada (NSERC), Strategic Project Grant no. 463045-14 led by the University of Guelph. We thank field assistants Terri Cheung and Bethany Ladd. Senior Technical Staff support from Robert Ingleton and Paul Johnson is greatly appreciated.

References

- Allen, D.T., V.M. Torres, J. Thomas, D.W. Sullivan, M. Harrison, A. Hendler, et al. 2013. Measurements of methane emissions at natural gas production sites in the United States. *Proc. Natl. Acad. Sci.* 110:17768–17773. doi:10.1073/pnas.1304880110
- Allen-King, R.M., R.M. Halket, D.R. Gaylord, and M.J.L. Robin. 1998. Characterizing the heterogeneity and correlation of perchloroethene sorption and hydraulic conductivity using a facies-based approach. *Water Resour. Res.* 34:385–396. doi:10.1029/97WR03496
- Alm, J., N.J. Shurpali, M. Maljanen, E.-S. Tuittila, K. Minkkinen, T. Laurila, and S. Saarnio. 2007. Methods for determining emission factors for the use of peat and peatlands: Flux measurements and modelling. *Boreal Environ. Res.* 12:85–100.
- Amos, R.T., K.U. Mayer, B.A. Bekins, G.N. Delin, and R.L. Williams. 2005. Use of dissolved and vapor-phase gases to investigate methanogenic degradation of petroleum hydrocarbon contamination in the subsurface. *Water Resour. Res.* 41:W02001. doi:10.1029/2004WR003433
- Bachu, S. 2017. Analysis of gas leakage occurrence along wells in Alberta, Canada, from a GHG perspective: Gas migration outside well casing. *Int. J. Greenhouse Gas Control* 61:146–154. doi:10.1016/j.ijggc.2017.04.003
- Baird, A.J., C.W. Beckwith, S. Waldron, and J.M. Waddington. 2004. Ebullition of methane-containing gas bubbles from near-surface *Sphagnum* peat. *Geophys. Res. Lett.* 31:L21505. doi:10.1029/2004GL021157
- Bird, M.I., and P. Pousai. 1997. Variations of d¹³C in the surface soil organic carbon pool. *Global Biogeochem. Cycles* 11:313–322. doi:10.1029/97GB01197
- Bogner, J.E., K.A. Spokas, and E.A. Burton. 1997. Kinetics of methane oxidation in a landfill cover soil: Temporal variations, a whole-landfill oxidation experiment, and modeling of net CH₄ emissions. *Environ.*

- Sci. Technol. 31:2504–2514. doi:10.1021/es960909a
- Boothroyd, I.M., S. Almond, S.M. Qassim, F. Worrall, and R.J. Davies. 2016. Fugitive emissions of methane from abandoned, decommissioned oil and gas wells. *Sci. Total Environ.* 547:461–469. doi:10.1016/j.scitotenv.2015.12.096
- Cahill, A.G., B.L. Parker, B. Mayer, K.U. Mayer, and J.A. Cherry. 2018. High resolution spatial and temporal evolution of dissolved gases in groundwater during a controlled natural gas release experiment. *Sci. Total Environ.* 622–623:1178–1192. doi:10.1016/j.scitotenv.2017.12.049
- Cahill, A.G., C.M. Steelman, O. Forde, O. Kuloyo, S.E. Ruff, B. Mayer, et al. 2017. Mobility and persistence of methane in groundwater in a controlled-release field experiment. *Nat. Geosci.* 10:289–294. doi:10.1038/ngeo2919
- Castro, M.S., P.A. Steudler, J.M. Melillo, J.D. Aber, and R.D. Bowden. 1995. Factors controlling atmospheric methane consumption by temperate forest soils. *Global Biogeochem. Cycles* 9:1–10. doi:10.1029/94GB02651
- Caulton, D.R., P.B. Shepson, R.L. Santoro, J.P. Sparks, R.W. Howarth, A.R. Ingraffea, et al. 2014. Toward a better understanding and quantification of methane emissions from shale gas development. *Proc. Natl. Acad. Sci.* 111:6237–6242. doi:10.1073/pnas.1316546111
- Council of Canadian Academies. 2014. Environmental impacts of shale gas extraction in Canada. Expert Panel on Harnessing Science and Technology to Understand the Environmental Impacts of Shale Gas Extraction, Council of Canadian Academies, Ottawa, ON.
- Chamindu Deepagoda, T.K.K., K.M. Smits, and C.M. Oldenburg. 2016. Effect of subsurface soil moisture variability and atmospheric conditions on methane gas migration in shallow subsurface. *Int. J. Greenhouse Gas Control* 55:105–117. doi:10.1016/j.ijggc.2016.10.016
- Dai, J., Y. Ni, D. Gong, Z. Feng, D. Liu, W. Peng, and W. Han. 2017. Geochemical characteristics of gases from the largest tight sand gas field (Sulige) and shale gas field (Fuling) in China. *Mar. Pet. Geol.* 79:426–438. doi:10.1016/j.marpetgeo.2016.10.021
- Darrah, T.H., A. Vengosh, R.B. Jackson, N.R. Warner, and R.J. Poreda. 2014. Noble gases identify the mechanisms of fugitive gas contamination in drinking-water wells overlying the Marcellus and Barnett Shales. *Proc. Natl. Acad. Sci.* 111:14076–14081. doi:10.1073/pnas.1322107111
- Davies, R.J., S. Almond, R.S. Ward, R.B. Jackson, C. Adams, F. Worrall, et al. 2014. Oil and gas wells and their integrity: Implications for shale and unconventional resource exploitation. *Mar. Pet. Geol.* 56:239–254. <https://doi.org/10.1016/j.marpetgeo.2014.03.001>
- Delahaye, C.H., and E.A. Pérez de Agreda. 2002. Soil heterogeneity and preferential paths for gas migration. *Eng. Geol.* 64(2). doi:10.1016/S0013-7952(01)00104-1
- Dusseault, M., M. Gray, and P. Nawrocki. 2000. Why oilwells leak: Cement behavior and long-term consequences. In: International Oil and Gas Conference and Exhibition in China, Beijing, 7–10 Nov. 2000. Soc. Pet. Eng., Richardson, TX. doi:10.2118/64733-MS
- Dusseault, M., and R. Jackson. 2014. Seepage pathway assessment for natural gas to shallow groundwater during well stimulation, in production, and after abandonment. *Environ. Geosci.* 21(3):107–126. doi:10.1306/eg.04231414004
- Erno, B., and R. Schmitz. 1996. Measurements of soil gas migration around oil and gas wells in the Lloydminster area. *J. Can. Pet. Technol.* 35(7). doi:10.2118/96-07-05
- Esposito, A. 2014. Migration of natural gas through heterogeneous sandy soils affected by atmospheric boundary conditions. In: Unconventional Resources Technology Conference, Denver, CO. 25–27 Aug. 2014. Aust. Soc. Exploration Geophys., NSW, Australia. doi:10.15530/urtec-2014-1937753
- Ferbey, T., A.S. Hickin, T.E. Demchuck, and V.M. Levson. 2008. Northeast British Columbia Aggregate Mapping Program: A summary of selected aggregate occurrences northeast of Fort Nelson. Ministry of Energy and Mines, Vancouver, BC, Canada.
- Forbrich, I., L. Kutzbach, A. Hormann, and M. Wilmking. 2010. A comparison of linear and exponential regression for estimating diffusive CH₄ fluxes by closed-chambers in peatlands. *Soil Biol. Biochem.* 42:507–515. doi:10.1016/j.soilbio.2009.12.004
- Golding, S.D., C.J. Boreham, and J.S. Esterle. 2013. Stable isotope geochemistry of coal bed and shale gas and related production waters: A review. *Int. J. Coal Geol.* 120:24–40. doi:10.1016/j.coal.2013.09.001
- Gorody, A.W. 2012. Factors affecting the variability of stray gas concentration and composition in groundwater. *Environ. Geosci.* 19(1):17–31. doi:10.1306/eg.12081111013
- Hammond, P.A. 2015. The relationship between methane migration and shale-gas well operations near Dimock, Pennsylvania, USA. *Hydrogeol. J.* 24:503–519. doi:10.1007/s10040-015-1332-4
- Harrison, S.S. 1983. Evaluating system for ground-water contamination hazards due to gas-well drilling on the glaciated Appalachian plateau. *Ground Water* 21:689–700. doi:10.1111/j.1745-6584.1983.tb01940.x
- Harrison, S.S. 1985. Contamination of aquifers by overpressuring the annulus of oil and gas wells. *Ground Water* 23:317–324. doi:10.1111/j.1745-6584.1985.tb00775.x
- Heijmans, M.M., P.D. Arp, and F.S. Chapin. 2004. Carbon dioxide and water vapour exchange from understory species in boreal forest. *Agric. For. Meteorol.* 123(3):135–147. doi:10.1016/j.agrformet.2003.12.006
- Humez, P., B. Mayer, J. Ing, M. Nightingale, V. Becker, A. Kingston, et al. 2016. Occurrence and origin of methane in groundwater in Alberta (Canada): Gas geochemical and isotopic approaches. *Sci. Total Environ.* 541:1253–1268. doi:10.1016/j.scitotenv.2015.09.055
- Jackson, R.B., A. Vengosh, J.W. Carey, R.J. Davies, T.H. Darrah, F. O'Sullivan, and G. Pétron. 2014. The environmental costs and benefits of fracking. *Annu. Rev. Environ. Resour.* 39:327–362. doi:10.1146/annurev-environ-031113-144051
- Jackson, R.B., A. Vengosh, T.H. Darrah, N.R. Warner, A. Down, R.J. Poreda, et al. 2013. Increased stray gas abundance in a subset of drinking water wells near Marcellus shale gas extraction. *Proc. Natl. Acad. Sci.* 110:11250–11255. doi:10.1073/pnas.1221635110
- Johnson, M.R., D.R. Tyner, S. Conley, S. Schwietzke, and D. Zavala-Araiza. 2017. Comparisons of airborne measurements and inventory estimates of methane emissions in the Alberta upstream oil and gas sector. *Environ. Sci. Technol.* 51:13008–13017. doi:10.1021/acs.est.7b03525
- Johnson, R.L., P.C. Johnson, D.B. McWhorter, R.E. Hinchee, and I. Goodman. 1993. An overview of in situ air sparging. *Groundwater Monit. Rem.* 13:127–135. doi:10.1111/j.1745-6592.1993.tb00456.x
- Kang, M., S. Christian, M.A. Celia, D.L. Mauzerall, M. Bill, A.R. Miller, et al. 2016. Identification and characterization of high methane-emitting abandoned oil and gas wells. *Proc. Natl. Acad. Sci.* 113:13636–13641. doi:10.1073/pnas.1605913113
- Kim, D.-G., R. Vargas, B. Bond-Lamberty, and M.R. Turetsky. 2012. Effects of soil rewetting and thawing on soil gas fluxes: A review of current literature and suggestions for future research. *Biogeosciences* 9:2459–2483. doi:10.5194/bg-9-2459-2012
- Lan, X., R. Talbot, P. Laine, and A. Torres. 2015. Characterizing fugitive methane emissions in the Barnett Shale area using a mobile laboratory. *Environ. Sci. Technol.* 49:8139–8146. doi:10.1021/es5063055
- Law, B.E., F.M. Kelliher, D.D. Baldocchi, P.M. Anthoni, J. Irvine, D. Moore, and S. Van Tuyl. 2001. Spatial and temporal variation in respiration in a young ponderosa pine forest during a summer drought. *Agric. For. Meteorol.* 110:27–43. doi:10.1016/S0168-1923(01)00279-9
- LI-COR. 2015. LI-8100A Automated soil CO₂ flux system & LI-8150 multiplexer instruction manual. LI-COR, Lincoln, NE.
- Mason, E.A., and A.P. Malinauskas. 1983. Gas transport in porous media: The dusty-gas model. Elsevier, Amsterdam.
- McCray, J.E., and R.W. Falta. 1996. Defining the air sparging radius of influence for groundwater remediation. *J. Contam. Hydrol.* 24:25–52. doi:10.1016/0169-7722(96)00005-8
- Millington, R.J. 1959. Gas diffusion in porous media. *Science* 130:100–102. doi:10.1126/science.130.3367.100-a
- Molins, S., and K.U. Mayer. 2007. Coupling between geochemical reactions and multicomponent gas and solute transport in unsaturated media: A reactive transport modeling study. *Water Resour. Res.* 43:W05435. doi:10.1029/2006WR005206
- Molins, S., K.U. Mayer, C. Scheutz, and P. Kjeldsen. 2008. Transport and reaction processes affecting the attenuation of landfill gas in cover soils. *J. Environ. Qual.* 37:459–468. doi:10.2134/jeq2007.0250

- Molins, S., K.U. Mayer, R.T. Amos, and B.A. Bekins. 2010. Vadose zone attenuation of organic compounds at a crude oil spill site: Interactions between biogeochemical reactions and multicomponent gas transport. *J. Contam. Hydrol.* 112:15–29. doi:10.1016/j.jconhyd.2009.09.002
- Mumford, K.G., J.E. Smith, and S.E. Dickson. 2010. The effect of spontaneous gas expansion and mobilization on the aqueous-phase concentrations above a dense non-aqueous phase liquid pool. *Adv. Water Resour.* 33:504–513. doi:10.1016/j.advwatres.2010.02.002
- Myhre, G.D., F.M. Shindell, and W. Breon. 2013. Anthropogenic and natural radiative forcing. In: T.F. Stocker et al., editors, *Climate change 2013: The physical science basis. Working Group I Contribution to the Fifth Assessment Report of the Intergovernmental Panel on Climate Change.* Cambridge Univ. Press, Cambridge, UK. p. 659–740. doi:10.1017/CBO9781107415324.018
- Nowamooz, A., J.-M. Lemieux, J. Molson, and R. Therrien. 2015. Numerical investigation of methane and formation fluid leakage along the casing of a decommissioned shale gas well. *Water Resour. Res.* 51:4592–4622. doi:10.1002/2014WR016146
- Osborn, S.G., A. Vengosh, N.R. Warner, and R.B. Jackson. 2011. Methane contamination of drinking water accompanying gas-well drilling and hydraulic fracturing. *Proc. Natl. Acad. Sci.* 108:8172–8176. doi:10.1073/pnas.1100682108
- Pihlatie, M.K., J.R. Christiansen, H. Aaltonen, J.F.J. Korhonen, A. Nordbo, T. Rasilo, et al. 2013. Comparison of static chambers to measure CH₄ emissions from soils. *Agric. For. Meteorol.* 171–172:124–136. doi:10.1016/j.agrformet.2012.11.008
- Revesz, K., T.B. Coplen, M.J. Baedeker, P.D. Glynn, and M. Hult. 1995. Methane production and consumption monitored by stable H and C isotope ratios at a crude oil spill site, Bemidji, Minnesota. *Appl. Geochem.* 10:505–516. doi:10.1016/0883-2927(95)00021-6
- Rey, A., C. Oyonarte, T. Morán-López, J. Raimundo, and E. Pegoraro. 2017. Changes in soil moisture predict soil carbon losses upon rewetting in a perennial semiarid steppe in SE Spain. *Geoderma* 287:2959–2975. doi:10.1016/j.geoderma.2016.06.025
- Rice, A.K., J.E. McCray, and K. Singha. 2018. Methane leakage from hydrocarbon wellbores into overlying groundwater: Numerical investigation of the multiphase flow processes governing migration. *Water Resour. Res.* 54:2959–2975. doi:10.1002/2017WR021365
- Roy, N., J. Molson, J.-M. Lemieux, D. Van Stempvoort, and A. Nowamooz. 2016. Three-dimensional numerical simulations of methane gas migration from decommissioned hydrocarbon production wells into shallow aquifers. *Water Resour. Res.* 52:5598–5618. doi:10.1002/2016WR018686
- Scheutz, C., and P. Kjeldsen. 2004. Environmental factors influencing attenuation of methane and hydrochlorofluorocarbons in landfill cover soils. *J. Environ. Qual.* 33:72–79. doi:10.2134/jeq2004.7200
- Selker, J.S., M. Niemet, N.G. McDuffie, S.M. Gorelick, and J.-Y. Parlange. 2006. The local geometry of gas injection into saturated homogeneous porous media. *Transp. Porous Media* 68:107–127. doi:10.1007/s11242-006-0005-0
- Sihota, N.J., and K.U. Mayer. 2012. Characterizing vadose zone hydrocarbon biodegradation using carbon dioxide effluxes, isotopes, and reactive transport modeling. *Vadose Zone J.* 11(4). doi:10.2136/vzj2011.0204
- Sihota, N.J., K.U. Mayer, M.A. Toso, and J.F. Atwater. 2013. Methane emissions and contaminant degradation rates at sites affected by accidental releases of denatured fuel-grade ethanol. *J. Contam. Hydrol.* 151:1–15. doi:10.1016/j.jconhyd.2013.03.008
- Sihota, N.J., O. Singurindy, and K.U. Mayer. 2011. CO₂-efflux measurements for evaluating source zone natural attenuation rates in a petroleum hydrocarbon contaminated aquifer. *Environ. Sci. Technol.* 45:482–488. doi:10.1021/es1032585
- Steelman, C.M., D.R. Klazinga, A.G. Cahill, A.L. Endres, and B.L. Parker. 2017. Monitoring the evolution and migration of a methane gas plume in an unconfined sandy aquifer using time-lapse GPR and ERT. *J. Contam. Hydrol.* 205:12–24. doi:10.1016/j.jconhyd.2017.08.011
- Strack, M., E. Kellner, and J.M. Waddington. 2006. Effect of entrapped gas on peatland surface level fluctuations. *Hydrol. Processes* 20:3611–3622. doi:10.1002/hyp.6518
- Strack, M., and J.M. Waddington. 2008. Spatiotemporal variability in peatland subsurface methane dynamics. *J. Geophys. Res. Biogeosci.* 113:G02010. doi:10.1029/2007JG000472
- Sudicky, E.A., and W.A. Illman. 2011. Lessons learned from a suite of CFB Borden experiments. *Groundwater* 49:630–648. doi:10.1111/j.1745-6584.2011.00843.x
- Sudicky, E.A., W.A. Illman, I.K. Goltz, J.J. Adams, and R.G. McLaren. 2010. Heterogeneity in hydraulic conductivity and its role on the macroscale transport of a solute plume: From measurements to a practical application of stochastic flow and transport theory. *Water Resour. Res.* 46:W0150. doi:10.1029/2008WR007558
- Tomlinson, D.W., N.R. Thomson, R.L. Johnson, and J.D. Redman. 2003. Air distribution in the Borden aquifer during in situ air sparging. *J. Contam. Hydrol.* 67:113–132. doi:10.1016/S0169-7722(03)00070-6
- Trumbore, S. 2000. Age of soil organic matter and soil respiration: Radiocarbon constraints on belowground C dynamics. *Ecol. Appl.* 10:399–411. doi:10.1890/1051-0761(2000)010[0399:AOSOMA]2.0.CO;2
- Watson, T.L., and S. Bachu. 2009. Evaluation of the potential for gas and CO₂ leakage along wellbores. *SPE Drill. Completion* 24:115–126. doi:10.2118/106817-PA
- Whiticar, M.J., and E. Faber. 1986. Methane oxidation in sediment and water column environments: Isotope evidence. *Org. Geochem.* 10:759–768. doi:10.1016/S0146-6380(86)80013-4
- Xu, L., X. Lin, J. Amen, K. Welding, and D. McDermitt. 2014. Impact of changes in barometric pressure on landfill methane emission. *Global Biogeochem. Cycles* 28:679–695. doi:10.1002/2013GB004571
- Zhang, Y., T. Sachs, C. Li, and J. Boike. 2012. Upscaling methane fluxes from closed chambers to eddy covariance based on a permafrost biogeochemistry integrated model. *Global Change Biol.* 18:1428–1440. doi:10.1111/j.1365-2486.2011.02587.x